

ABSTRACT

Regional Elemental and Organic Geochemical Character of the Devonian/Mississippian Exshaw Formation across Alberta, Canada

Mason Norman Frucci, M.S.

Co-advisor: James M. Fulton, Ph.D.

Co-advisor: Stacy C. Atchley, Ph.D.

A regional geochemical study of the Devonian/Mississippian Exshaw shale across Alberta was conducted to test the hypothesis that the shale has widespread organic matter richness accompanied by redox-sensitive trace metal enrichment and biomarker ratios reflecting widespread, consistent anoxia. Our dataset enables a multi-proxy investigation of depositional environments and thermal maturity using whole-rock samples taken from 20 locations across southern and central Alberta. Rock-Eval 7S, Handheld XRF and GC-MS are used in concert to conclude that the Exshaw shale is within the oil window for much of its geographical area. The organic matter is oil-prone, marine producer-sourced, moderately sulfur-rich (Type IIS, HI>400), and of excellent kerogen quality (TOC>2%, S₂>10) where not overmature. Biomarker ratios and trace metal concentrations suggest that although reducing conditions were consistent throughout deposition, anoxia varied across the basin. Biomarker thermal maturity proxies generally agree with T_{max} values that thermal maturity increases southwestward.

Regional Elemental and Organic Geochemical Character of the Devonian/Mississippian Exshaw
Formation across Alberta, Canada

by

Mason Norman Frucci, B.S.

A Thesis

Approved by the Department of Geosciences

Joe C. Yelderman, Jr. Ph.D., Chairperson

Submitted to the Graduate Faculty of
Baylor University in Partial Fulfillment of the
Requirements for the Degree
of
Master of Science

Approved by the Thesis Committee

James M. Fulton, Ph.D., Co-chairperson

Stacy C. Atchley, Ph.D., Co-chairperson

Rebecca J. Sheesley, Ph.D.

Accepted by the Graduate School

August 2021

J. Larry Lyon, Ph.D., Dean

Copyright © 2021 by Mason Norman Frucci

All rights reserved

TABLE OF CONTENTS

LIST OF FIGURES	v
LIST OF TABLES	vi
ACKNOWLEDGMENTS	vii
DEDICATION	viii
CHAPTER ONE	1
Introduction	1
<i>Overview</i>	1
<i>Background</i>	3
CHAPTER TWO	9
Methods and Samples	9
<i>Samples</i>	9
<i>Analytical Methods</i>	10
CHAPTER THREE	18
Results	18
<i>Elemental Geochemistry</i>	18
<i>Rock-Eval Pyrolysis</i>	26
<i>n-Alkanes and Biomarkers</i>	29
CHAPTER FOUR	35
Discussion	35
<i>Stratigraphy</i>	35
<i>Depositional Environment</i>	36
<i>Organic Matter Source</i>	46
<i>Source Rock Attributes</i>	54
CHAPTER FIVE	60
Conclusions	60
REFERENCES	62

LIST OF FIGURES

Figure 1. Basemap and paleogeography of the Exshaw Formation.....	4
Figure 2. Stratigraphic column for the Exshaw Formation.....	5
Figure 3. Molybdenum vs TOC crossplot.....	19
Figure 4. Redox-sensitive element stratigraphic profiles for three locations	20
Figure 5. Boxplots of elemental geochemistry for the Exshaw Shale Member.....	22
Figure 6. Scatterplots of aluminum versus elements of interest	24
Figure 7. Pie charts of elemental enrichment factors for redox-sensitive elements	25
Figure 8. Extracted ion chromatograms	29-30
Figure 9. Organic compound identities of chromatogram peaks	31
Figure 10. TS vs TOC crossplot	43
Figure 11. TOC-Fe-TS ternary diagram	44
Figure 12. CPI vs OEP crossplot	47
Figure 13. Pr/nC ₁₇ vs Ph/nC ₁₈ crossplot	49
Figure 14. Pseudo van Krevelen plot (HI vs OI)	52
Figure 15. Kerogen Quality plot (S ₂ vs TOC).....	55
Figure 16. Thermal maturity contour map with kerogen qualities	57
Figure 17. %20S vs % $\alpha\beta$ steranes crossplot	59

LIST OF TABLES

Table 1. Handheld XRF accuracy and precision from standards.....	13
Table 2. Rock Eval data from Exshaw Shale Member organic samples	27
Table 3. Elemental data from Exshaw Shale Member organic samples.....	28
Table 4. Organic molecular data from Exshaw Shale Member organic samples	33
Table 5. Redox-sensitive element proxy ratios for oxygen availability	40

ACKNOWLEDGMENTS

I am grateful to Dr. Jamey Fulton and Dr. Stacy Atchley for their guidance, training, expertise, and encouragement as co-advisors of this project, Julia Visy, Elizabeth Rau, Anna Thorson and Bart Yeates for their work in sample collection, Dr. Bill Hockaday for the use of his lab equipment and materials, Dr. Steve Dworkin for training and the use of his lab instrument, Wayne Hamilton and Dr. Joe Yeldermann for consistent smiles, encouragement and motivation, Dr. Mike Arthur for sharing his expertise on sulfur preservation, Kevin Bohacs for his suggestions on sample cleaning procedure, Humberto Carvajal-Ortiz for his expertise on Rock-Eval parameters, the Geosciences Department for their Graduate Research Grant, and the Geosciences Department front office staff for keeping everything in order. I am grateful also to Harris Creek Baptist Church and my Lifegroup there, my fantastic roommates Wynne Casteel, Stephen Curren and Cody Ross, the boys and guides of Heart of Texas Field Guides, Evan Jones, Cameron Lee, my aunts, my uncles, my cousins, Nana, Papa, Mimi, Pawpaw, my Mom, my Dad, and Reido Frucci.

DEDICATION

To Mom.

For instilling in me that His plans are good even when they confuse us, and that
Jesus' grace and salvation cannot be earned, only accepted.

CHAPTER ONE

Introduction

Overview

The Devonian/Mississippian Exshaw Formation consists of fine-grained siliciclastic/carbonate mudrock enriched in organic matter (OM) and is one of the black shale intervals with widespread deposition in the Western Canada Sedimentary Basin (WCSB; Macqueen and Sandberg, 1970; Richards et al., 1994; Richards and Higgins, 1988; Rokosh et al., 2012; Savoy, 1992; Smith and Bustin, 2000). The Exshaw occurs in the subsurface across much of Alberta and crops out in the fold and thrust belt on the western margin of the province (Figure 1). OM-rich mudrocks are important hydrocarbon source rocks for conventional petroleum reservoirs, unconventional reservoir targets, stratigraphic marker beds, and repositories of OM for paleoenvironmental investigations (Adams et al., 2013; Berbesi et al., 2012; Creaney and Allan, 1990; Fowler, 2001; Klemme and Ulmishek, 1991; McCarthy et al., 2011; Rokosh et al., 2012; Smith and Bustin, 2000). The broad geographic presence and OM-richness of this formation warrants an investigation into the variation in organic and elemental character of the formation on a regional scale.

The objective of this project is to investigate relationships between whole rock geochemistry and OM characteristics to test the hypothesis that the Exshaw Shale has widespread OM-richness that is accompanied by redox-sensitive trace metal enrichment and biomarker ratios that reflect widespread, consistent anoxia. These attributes have

been evaluated in previous studies with fewer locations or fewer proxies (e.g., Caplan and Bustin, 1996, 2001; Robison, 1995; Savoy, 1992; Yang, 2019), and this study expands on these earlier works to provide a better understanding on a regional scale. Twenty locations were chosen from southern and western Alberta to characterize the formation from a spatial standpoint across a broad region of its accumulation in the WCSB (Figure 1). The study reports primarily on the Exshaw Shale Member (Figure 2; Macqueen and Sandberg, 1970; Richards and Higgins, 1988), the most OM-rich unit of the formation, and presents geochemical averages, trends, and extremes. The deposition of this unit occurred over a geologically short duration (Creaser et al., 2002; Meijer Drees and Johnston, 1996), and its analysis may offer insight into variable biogeochemical conditions across the basin during deposition. Findings of this study have implications to both hydrocarbon production, and the diagenetic history and regional paleoenvironmental reconstruction at and around the time of the end-Devonian mass extinction (Caplan and Bustin, 1999; Martinez et al., 2019; Piszczowska et al., 2020). This laterally extensive fine-grain marine mudrock is one of several OM-rich shales across North America deposited during the end-Devonian, i.e., the Bakken Shale, Woodford Shale, and New Albany Shale formations. Geochemical attributes on a regional scale have implications for not only this formation, but also hydrocarbon-bearing reservoirs and the several concurrently deposited shales across the globe (Caplan and Bustin, 1999; Creaney and Allan, 1990; Creaser et al., 2002; Richards and Higgins, 1988; Robison, 1995; Savoy, 1990; Smith and Bustin, 2000).

Background

The Exshaw Formation was deposited during a latest Devonian and earliest Mississippian marine transgression and sea level high-stand in both the WCSB of Alberta and connected Williston Basin to the southeast in North Dakota, where the Bakken Formation was contemporaneously deposited (Creaney and Allan, 1990; Richards et al., 1994; Smith et al., 1995). Similar OM-rich shales were deposited at the Devonian/Carboniferous boundary across much of both North America and the world and account for a large portion of the world's hydrocarbon source rocks (Caplan and Bustin, 1999; Creaney and Allan, 1990; Kaiser et al., 2016; Klemme and Ulmishek, 1991; Peters et al., 2005b). The Exshaw Formation is an important source to both light and heavy-oil conventional and unconventional hydrocarbon reservoirs across the WCSB including the Lower Cretaceous Mannville Group adjacent the Peace River of western Alberta, and the Athabasca and Cold Lake oil sands of northeastern Alberta (Adams et al., 2013; Berbesi et al., 2012; Creaney and Allan, 1991; Karavas et al., 1998; Richards et al., 1994; Robison, 1995; Rokosh et al., 2012). The Exshaw Formation varies in total thickness from 3–40 m, with the Shale Member averaging 3 m in thickness (Caplan, 1997; Peters et al., 2005b). The Exshaw dips southwesterly and is truncated to a zero-thickness edge beneath Cretaceous strata along its northeastern boundary (Figure 1; Richards et al., 1994). Outcrops of the Exshaw Formation occur within the Rocky Mountain (Laramide-age) fold-and-thrust belt located in southwestern Alberta (Macqueen and Sandberg, 1970; Richards et al., 1994).

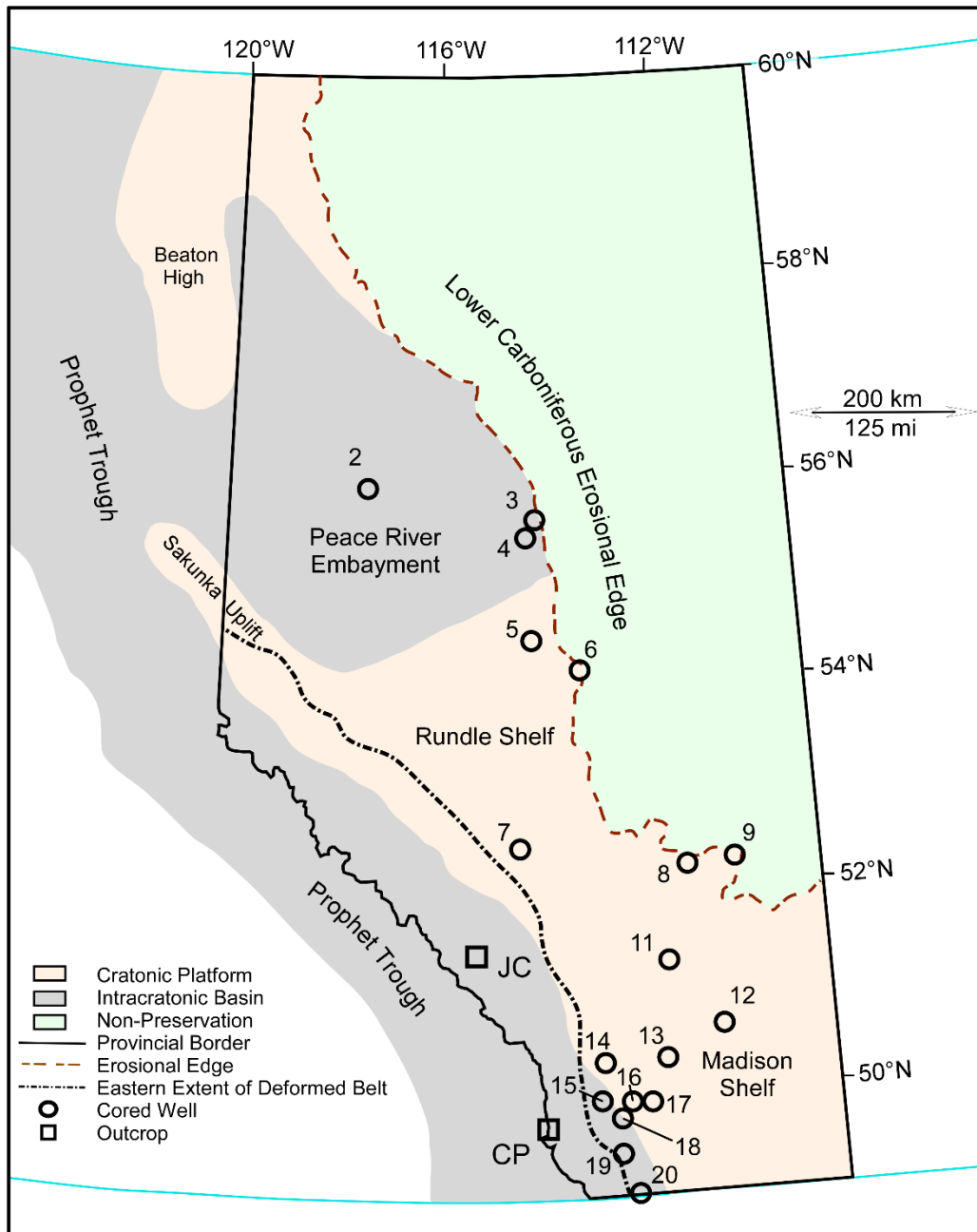


Figure 1. Map of the province of Alberta displaying the 20 locations of cores and outcrops investigated for this study. All logs were accessed through geoLOGIC Systems' geoSCOUT software. The location of paleogeographic features are from Richards (1989).

The Exshaw Formation consists of two lithologic members (Figure 2): the clay dominated Exshaw Shale and the overlying Siltstone Member (Macqueen and Sandberg, 1970). Within some areas the Exshaw Shale is subdivided into three units: a centimeter-

scale basal sandstone abruptly overlain by the “Lower Shale” and “Upper Shale” units (Richards and Higgins, 1988). The total organic carbon (TOC) content is consistently greater than 2% by weight for the Shale Member throughout the basin, with values commonly exceeding 10% and maximum reported values as high as 20% (Caplan and Bustin, 1996, 1998, 2001; Robison, 1995). The Exshaw Shale is the most TOC enriched member of the Exshaw Formation (Caplan and Bustin, 1996, 1998; Robison, 1995; Savoy, 1992), and the multi-core study by Robison (1995) on the Exshaw’s source rock attributes concluded that all of the formation’s hydrocarbon source potential was exclusive to the Exshaw Shale member.

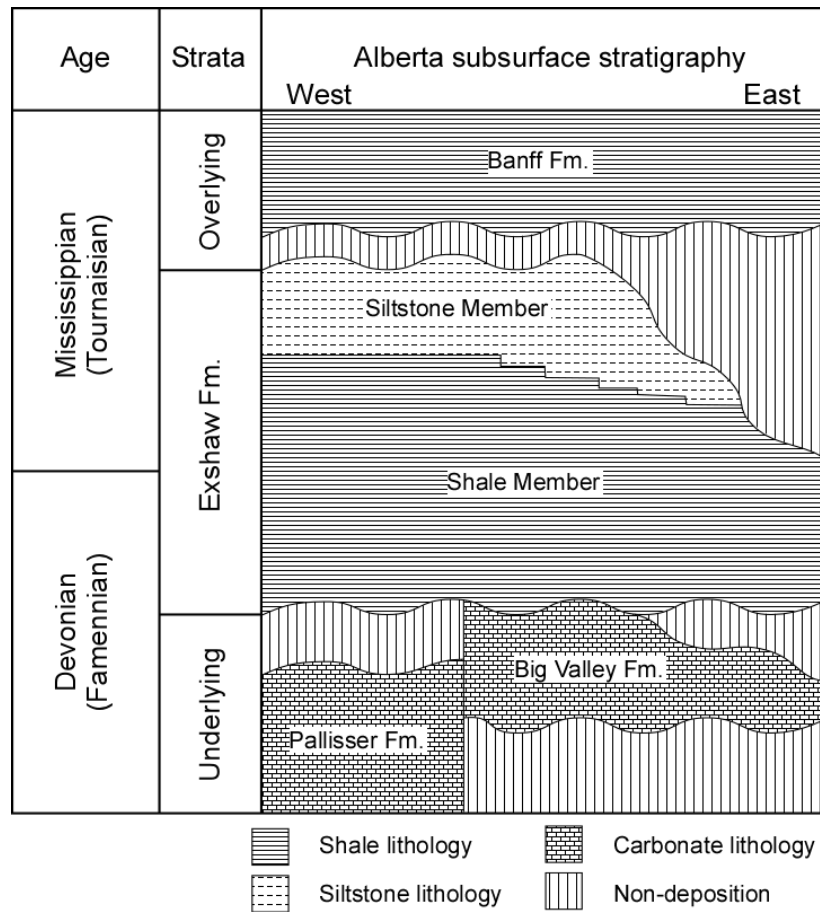


Figure 2. Simplified stratigraphic column for the Exshaw Formation within Alberta. Modified from Caplan and Bustin (2001), Richards et al. (1994) and Savoy (1990).

The Exshaw Shale is a transgressive deposit overlying the Acadian unconformity (Richards, 1989; Wheeler, 1963). The associated rise in eustatic sea level drowned carbonate production and resulted in a depositional hiatus between the underlying carbonates and Exshaw Shale (Caplan and Bustin, 1996, 2001; Creaney and Allan, 1990; Meijer Drees and Johnston, 1996). A thin (1-4 cm) sandstone lag deposit is present at the base of the Exshaw Formation in some locations (Macqueen and Sandberg, 1970; Richards and Higgins, 1988; Savoy, 1992; Smith and Bustin, 2000) and is utilized as a stratigraphic marker bed where present.

Basin bathymetry during accumulation was primarily controlled by the tectonic influences on the downwarped North American plate (Richards, 1989; Richards et al., 1994) that formed the paleogeographic features depicted in Figure 1. Paleogeographic highs and lows produced from basement block faulting have been proposed as a possible cause for thickness variations in the southern portion of Alberta (Caplan and Bustin, 1996). Deposition occurred in low paleolatitudes within 10°S-15°N (Scotese and McKerrow, 1990; Witzke and Heckel, 1988; Witzke, 1990) in warm waters of an epeiric seaway across the intracratonic basin (Richards, 1989; Savoy, 1992; Witzke and Heckel, 1988). Algeo et al. (2007) and Caplan and Bustin (1998) suggest that water body restriction affected depositional conditions across the WCSB during the end Devonian and early Mississippian (Algeo et al., 2007; Caplan and Bustin, 1998), including the possible silling by a hydrographic barrier to the west that impeded flow between the open ocean and epeiric seaway (Savoy and Mountjoy, 1995). Caplan and Bustin (1998, 2001) propose the westerly barrier to have been in place before and after Exshaw Shale deposition. Prior to Exshaw deposition, the sill created shallow, warm marine water

conditions concurrent with deposition of the Big Valley Limestone. The transgression increased water depth and connected the seaway to the ocean during accumulation of the Exshaw Shale. During the ensuing sea level fall, sea level dropped below the sill causing hydrographic isolation during deposition of the Exshaw Siltstone Member. Algeo et al. (2007) suggest that during restriction the north was more restricted than the south based on Mo/TOC ratios observed in single cores from each region. Recent work by (Yang, 2019) with trace metals and isotopes (molybdenum and sulfur) concludes that little to no deep-water restriction was occurring in the Peace River Embayment area. The most widely accepted primary mechanism for Shale Member organic enrichment and preservation is widespread upwelling along the coastal margins of the basin (Parrish, 1982; Savoy, 1992; Witzke, 1990). It is speculated that when the transgression overcame the hydrographic barrier (prior to Exshaw Shale accumulation), a nutrient-rich upwelling cell was introduced into the seaway and resulted in reducing bottom waters and accumulation and preservation of OM. The abundance of nutrients from upwelling water increased primary productivity and caused an anoxic water column (Caplan and Bustin, 1996, 1998, 2001). More specifically, increased photic-zone production of OM both increased organic carbon flux to the seafloor and depletion of oxygen through respiration. The degree of anoxia and water column stratification are debated, but it is generally accepted that bottom waters were suboxic to euxinic with the redoxcline above the sediment/water interface throughout deposition of the Exshaw Shale as suggested by organic richness, redox-sensitive trace metal enrichment, and preservation of planar laminations that indicate a lack of biogenic reworking of the sediment (Algeo et al., 2007; Caplan and Bustin, 1996, 1998, 2001; Macqueen and Sandberg, 1970; Meijer Drees and

Johnston, 1996; Richards and Higgins, 1988; Robison, 1995; Ross and Bustin, 2009; Savoy, 1992; Yang, 2019). The preservation of suspension lamina also suggests that the Exshaw Shale accumulated below storm wave base, perhaps on the continental shelf or slope (Caplan and Bustin, 1996, 1998, 2001; Richards and Higgins, 1988). Caplan and Bustin (1996) proposed the source of silt to be gravity flows off paleogeographic highs which also introduced oxygenated water into the anoxic layer. These pulses of oxygen to an otherwise anoxic seafloor degraded deposited OM in interspersed clay and silt laminae.

Thermal maturity of the Exshaw Formation across the WCSB increases to the southwest, from immature ($T_{max} < 430\text{ }^{\circ}\text{C}$) in the northeast to the dry gas zone ($T_{max} > 480\text{ }^{\circ}\text{C}$) in the Rocky Mountain foothills (Creaney and Allan, 1990; Richards et al., 1994; Robison, 1995; Rokosh et al., 2012; Yang, 2019). Despite wide variation in thermal maturity across the basin, previous studies have shown that trace metal concentrations in the Exshaw are not affected by thermal maturation (Creaser et al., 2002; Ross and Bustin, 2009; Yang, 2019).

CHAPTER TWO

Methods and Samples

Samples

Rock samples from 22 locations in the study area were investigated, including 20 cored intervals from wells and 2 outcrops (Figure 1). During data collection for this study, the Exshaw Formation was described and analyzed within continuous core from 18 wells (360 total meters) that are widely dispersed across the study area. Core were selected from wells where the Exshaw Shale Member has high gamma ray response suggestive of organic enrichment. Cored intervals from locations 1 and 10 did not include Exshaw formation and were not included in this study. In addition, 761 total points were analyzed by X-ray fluorescence (265 in the Exshaw Shale), and 47 samples were selected for OM characterization by Rock-Eval pyrolysis and gas chromatography/mass spectrometry (GC-MS). The cores were accessed at the Alberta Energy Regulator Core Research Centre in Calgary, Alberta. Well locations were included where core was completely recovered through the Exshaw Formation.

The Exshaw Shale Member was identified by use of wireline logs (accessed via geoLogic geoScout and IHS AccuMap software) to identify the Exshaw's diagnostic gamma ray (Rokosh et al., 2012), neutron and resistivity, and/or photoelectric log response. The specific wells were selected based on the conditions that they: (1) are geographically dispersed across the study area, (2) are reported in AccuMap and/or geoScout as having complete recovery through the Exshaw Shale, (3) upon initial

inspection and comparison with published type logs (e.g., Rokosh et al., 2012) inspire confidence that the cored interval is the Exshaw Shale Member, (4) are vertical wells, and (5) have modern (post-1980) well logs. Core from each location were described in detail and labeled with facies associations as differentiated based on ichnology, bioturbation, grain size, fossil prevalence, calcite reactivity to 10% HCl, fracture frequency, sedimentary structures and color. Each core was depth-corrected to match log depth through a comparison of core-observed rock attributes and gamma ray, induction, and/or neutron/density log response.

Whole rock samples from two outcrop locations, Jura Creek (51.076548, -115.181382) and Crowsnest Pass (49.625866, -114.648981), were collected from the rock face with hammer and chisel at 0.5 m resolution. A published outcrop description of the Exshaw type-section on Jura Creek by Richards and Higgins (1988) was used to establish unit boundaries and help guide sampling. The outcrop at Crowsnest Pass includes the exposure of the entire thickness of the Exshaw Formation (Macqueen and Sandberg, 1970). For ease of sample description, Jura Creek is referred to as “location 21” and Crowsnest Pass as “location 22” in some tables and figures.

Analytical Methods

X-Ray Fluorescence

Trace and major element concentrations were measured with a handheld Bruker TRACER 5i X-Ray Fluorescence (XRF) Spectrometer set to the internal Bruker *mudrock-dual* calibration. Portable energy-dispersive XRF is a fast and non-destructive alternative to laboratory-based wavelength-dispersive or energy-dispersive XRF

instruments and has sufficient precision for assessing changes in lithology, sediment sources, and depositional environments (Driskill et al., 2018; Martin and Carr, 2020; Rowe et al., 2012). Energy-dispersive analysis is widely used in industry and chemostratigraphic studies. Elemental concentrations were analyzed on a clean core surface (slabbed where possible) at 0.5 m. For this study uranium, molybdenum, vanadium, nickel and iron are used to assess redox conditions of depositional environments, and aluminum, silicon and calcium to evaluate sediment source (Calvert and Pedersen, 1993; Caplan and Bustin, 1998; Rimmer, 2004; Scott et al., 2017; Tribovillard et al., 2006). The reported limits (in weight %) of quantification for each element varied slightly with rock composition: Al 0.1%, Mg 0.15%, Si 0.03%, P 0.01%, S 0.03%, K 0.02%, Ca 0.1%, Ti 15ppm, V 8ppm, Cr 10ppm, Mn 25ppm, Fe 0.01%, Co 6ppm, Ni 18ppm, Cu 14ppm, Zn 8ppm, As 8ppm, Rb 5ppm, Sr 15ppm, Y 7ppm, Zr 5ppm, Nb 5ppm, Mo 6ppm, Ba 200ppm, Pb 9ppm, Th 4ppm, and U 15ppm. We report the percent composition as elemental concentration rather than as oxidized mineral phases. Thus, the reported elemental concentration for a given sample does not sum to 100%. A rock composed of 40% clay minerals, 30% silica and 30% calcium carbonate may theoretically produce the following readings (depending on clay composition): Al 3%; Si 20%; Ca 12% (silicon is ~46.7% of pure silica, calcium is ~40.0% of pure calcium carbonate, aluminum is <10% of most common clay minerals). Four standards, i.e., Zentrales Geologisches Institut *Black Shale* (ZGI TS), Mintek *Carbonaceous Shale* (SARM 41), Geological Survey of Japan *Black forest soil* (JSO-1), and Geological Survey of Japan *Porites sp. coral* (JCp-1), were analyzed at the beginning and end of each day of analysis to assess accuracy and precision and to produce calibration curves as

needed to correct for instrument instability. The reported concentration for each element used to assess reproducibility of our measured results is included in Table 1 along with measured mean concentration, 1σ standard deviation, coefficient of variation (CV), and percent error (%err) from our analysis.

$$\text{Coefficient of Variation (CV)} = \frac{\text{Standard Deviation of Measured Concentrations}}{\text{Mean of Measured Concentrations}}$$

$$\text{Percent Error (\%err)} = \left| \frac{\text{Reported Concentration} - \text{Mean of Measured Concentrations}}{\text{Reported Concentration}} \right|$$

The %err and CV for most elements are reported relative to the ZGI TS black shale standard because of similar lithology to our samples. The concentration of Ca, P, and S reported for ZGI TS was much lower than the values observed for Exshaw samples, so these elements are reported relative to the JSO-1 standard that has similar reported concentration. Prior to analyzing the final samples (Locations 13, 17, 18 and Crowsnest Pass outcrop), the instrument calibration shifted causing measured element concentrations to decrease and %err to increase, though CV did not change significantly (for example: ZGI TS Fe pre-shift %err = 16% and CV = 2%; ZGI TS Fe post-shift %err = 54% and CV = 4%). Calibration curves were made for each element using standards analyzed during this latter part of the sample run, and the resulting corrected mean and standard deviation values were similar to values for samples analyzed earlier.

Table 1. XRF data from analysis of international standards

Element	Standard	Reported Concentration (wt.%)	Mean of Measured Concentrations (wt.%)	Standard Deviation (wt.%)	CV (%)	%err (%)
Si	TS	29.33	19.73	1.68	9	33
Al	TS	8.44	7.48	0.76	10	11
Ca	JSO-1	1.83	1.57	0.13	8	14
P	JSO-1	0.21	0.13	0.01	10	38
Fe	TS	5.18	4.35	0.08	2	16
S	JSO-1	0.20	0.17	0.02	12	15
Cu	TS	0.0460	0.0527	0.0016	3	15
V	TS	0.0960	0.0786	0.0028	4	18
Ni	TS	0.0170	0.0191	0.0011	6	12
Mo	TS	0.0130	0.0096	0.0003	3	26
U	TS	0.0022	0.0032	0.0006	19	45

Elemental enrichment in this study is evaluated relative to the reference abundance values reported for the “Average Shale” (Wedepohl, 1971, 1995). These reference values for global average trace element content of shales are commonly applied in geochemical studies to facilitate comparison between samples from different environments, formations, and studies in the form of Enrichment Factors (EF),

$$EF_{X,sample} = (X/Al)_{sample} / (X/Al)_{AvShale}$$

where X and Al are the trace element and aluminum content, respectively, in the sample or average shale. Since trace element concentration is a function of both ocean chemistry at the time of deposition and detrital input, an EF accounts for the allochthonous metal enrichment caused from input of eroded continental detritus by normalizing values to aluminum concentration, assuming detrital trace elements correlate with Al (Calvert and Pedersen, 1993; Tribovillard et al., 2006).

Sample Preparation for Organic Matter Characterization

47 samples of the Exshaw Formation from 18 cores and two outcrops were analyzed by Rock Eval pyrolysis and GC-MS. Of those, 37 were from the Exshaw Shale Member and are included in this study. External surfaces of all samples were cleaned to remove surface contaminants from either drilling fluid and/or handling in the core lab (Peters et al., 2005a; Steiner and Grzegorz, 2016). Whole rock samples were broken with hammer and chisel to pebble-size fragments and submerged in 100% dichloromethane (DCM) for 10 minutes. The solvent was decanted, the rinse and decanting step was repeated, and the sample was allowed to dry in a fume hood. The fragments were then crushed in a ShatterBox (SPEX Industries Inc., Catalog No. 8500) and sealed in pre-combusted (460 °C, 6 h) glass jars. Between samples, the ShatterBox puck, ring, O-ring gasket, dish and lid were cleaned by grinding combusted quartz sand and then rinsing sequentially with organic-free detergent (Alconox Powdered Precision Cleaner), deionized water, methanol, DCM and acetone.

For GC-MS analysis, lipids were extracted from powdered sample using a Dionex ASE 200 Accelerated Solvent Extractor at 1000 psi and 100 °C with 9:1 DCM:methanol. The resulting total lipid extract was evaporated to near dryness using a Turbovap LV and taken up in 9:1 hexane:DCM. To remove water and elemental sulfur commonly present in shale extracts, activated copper wire and Na₂SO₄ were added to each vial and 0.1 mL of 5000 ppm deuterated n-eicosane (D42) was also added as an internal standard to normalize compound concentrations for comparison between samples. This mixture was evaporated in an N₂ stream to near dryness, taken up in 3 mL of hexane, and passed through a Pasteur pipette containing a combusted glass-wool-plug into a new combusted

vial to filter out the copper wire, Na_2SO_4 and asphaltenes. Open column chromatography was then performed using hexane-saturated activated silica gel in a 15-cm combusted glass-wool-plugged pipette. The extracts were evaporated down to 1 mL under N_2 and 0.3 mL were transferred to the head of the column and eluted first with 3 mL of 9:1 hexane:DCM and then with 3 mL of 8:2 hexane:DCM, collected in separate vials. Those fractions were concentrated to <0.1 mL in conical glass inserts in GC autosampler vials in preparation for analysis by GC-MS.

Rock-Eval Pyrolysis Parameters

Samples for Rock-Eval Pyrolysis were analyzed on a Vinci Technologies Rock-Eval 7S instrument (Core Laboratories, Houston, Texas). Rock-Eval 7S pyrolyzes organic matter in rock powders into three fractions distinguished on a pyrogram as S1 (“free hydrocarbon,” mg HC/g rock), S2 (hydrocarbon generative potential, mg HC/g rock), and S3 (organic-derived CO_2 , mg CO_2 /g rock). Additional measured parameters include TOC (total organic carbon, g TOC/g rock*100) and Tmax, (temperature of maximum hydrocarbon yield during pyrolysis, °C). Parameters derived from these data include OI (oxygen index= $\text{S3}/\text{TOC}$, mg CO_2 /g TOC), HI (hydrogen index= $\text{S2}/\text{TOC}$, mg HC/g TOC), and PI (production index = $\text{S1}/(\text{S1}+\text{S2})$). These parameters are described in detail by Peters (1986). Rock-Eval 7S also analyzes organic and mineral sulfur and reports TS (total sulfur, g S/g rock *100), TOS (total organic sulfur, g TOS/g rock *100), and Fe-S (inorganic sulfur residing in pyrite and other sulfide minerals, g S/g rock; Abousou et al., 2018; Vinci-Technologies, 2021). Presence of these sulfur species in petroleum source rocks offers insight to aspects of sulfur chemistry that relate to hydrocarbon yield and the quantity, quality, and thermal maturity of OM (Carvajal-Ortiz

and Gentzis, 2015; Peters, 1986). These data provide our project with industry-standard estimates that offer a more complete understanding of the system when used in conjunction with elemental and organic geochemical data.

Gas Chromatography-Mass Spectrometry

A Hewlett Packard HP 6890 Series GC System was used to analyze the non-polar fraction of total lipid extracts acquired through the column chromatography method described in a previous paragraph. The temperature program was set for a 70-minute run time, with a starting oven temperature of 70 °C ramping to 300 °C in two stages: 70-210 °C at 5 °C/min then 210-300 °C at 3 °C/min and holding at 300 °C for 10 minutes. We conducted splitless injection using helium at 8.80 psi, injector temperature 250 °C, and 1.0 mL/min through an Agilent 19091J-433 stationary-phase capillary column (30 m length, 250 µm outside thickness, 5% Phenyl Methyl Siloxane 0.25 µm film thickness). Data acquisition and analysis were done on Agilent Technologies Enhanced ChemStation software where the resulting chromatograms and integrated peak areas can be investigated. Compounds were identified by comparing relative peak positions to those in external standards (for n-alkanes, Supelco Analytical Catalog No. 49452-U; for hopanes and steranes, National Institute of Standards and Technology Standard Reference Material 2266; for whole rock extracts, United States Geological Survey SGR-1B). The relative compound abundance was calculated for use in biomarker ratios by integrating their peak areas on extracted ion chromatograms for the mass-to-charge (m/z) ratios: m/z 57 (n-alkanes), m/z 191 (hopanes), and m/z 217 (steranes). Deuterated n-eicosane (m/z

66) was used as an internal standard to normalize compound abundances for comparison of Relative Concentration (RC) between samples.

CHAPTER THREE

Results

Elemental Geochemistry

Black shales have high OM content and are typically enriched in trace metals relative to other upper crust lithologies (Vine and Tourtelot, 1970; Wedepohl, 1971, 1995) because the reducing, oxygen-limited conditions that allow for preservation of OM also favor insoluble reduced mineral phases that accumulate in anoxic sediments (Arthur and Sageman, 1994; Calvert and Pedersen, 1993; Hatch and Leventhal, 1992). Thus, redox-sensitive trace metals are often used as a predictor for OM content. In our samples, there is a positive correlation between molybdenum and TOC that illustrates this concept (Figure 3), and additional elemental concentrations and ratios are investigated for a more robust understanding of the system.

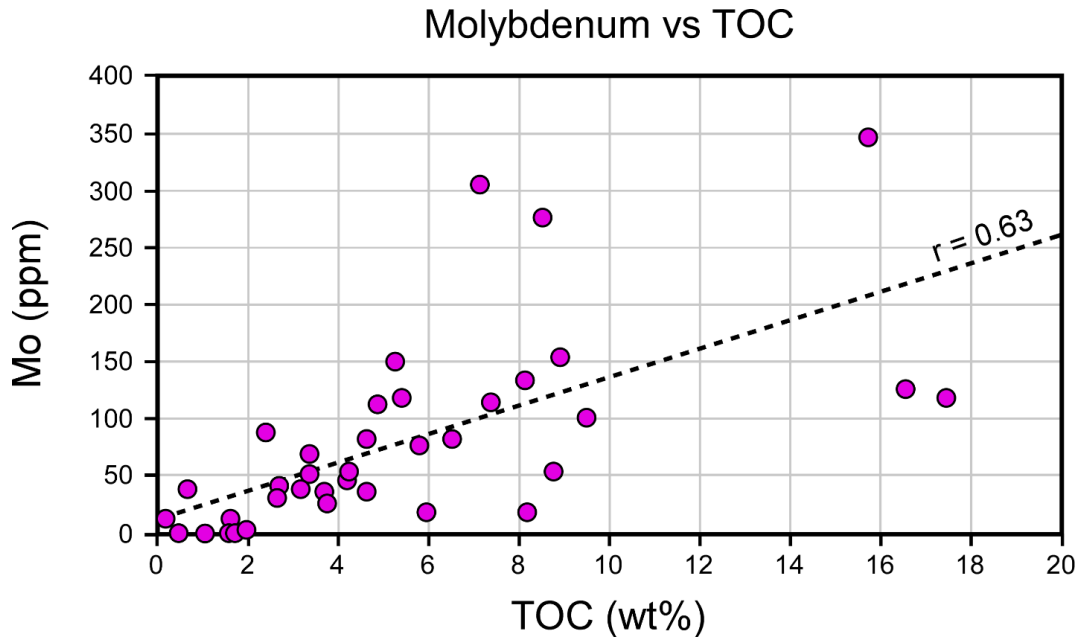


Figure 3. Crossplot showing the relationship between TOC and molybdenum in Exshaw shale samples.

The Exshaw Shale Member consists of black, laminated mudrock in nearly every location (exceptions: locations 15, 16, 18, and 19 had some massive bedding) whereas underlying strata of the Palliser Formation in central Alberta and the Big Valley Formation in southeast Alberta are characterized by open marine carbonates (Meijer Drees and Johnston, 1996; Richards et al., 1994). In our samples, the Exshaw Shale Member consistently has higher concentrations of redox-sensitive trace metals than the underlying limestone or overlying Siltstone Member (Figure 4) and is in agreement with observations provided in previous publications (Caplan and Bustin, 1996, 1998). This observation is consistent regardless of level of thermal maturity, and supports previous literature that found trace metals are relatively immobile irrespective of the level of catagenesis (Ross and Bustin, 2009). The magnitude of concentration discrepancy between members varies by location, but the Exshaw Shale Member consistently has higher concentrations relative to overlying and underlying strata (Figure 4). The Exshaw

Shale Member does not have one consistent stratigraphic enrichment pattern across the study area, rather, concentrations decrease upward at some locations (Figure 4A) and increase upward in others (Figure 4B and C).

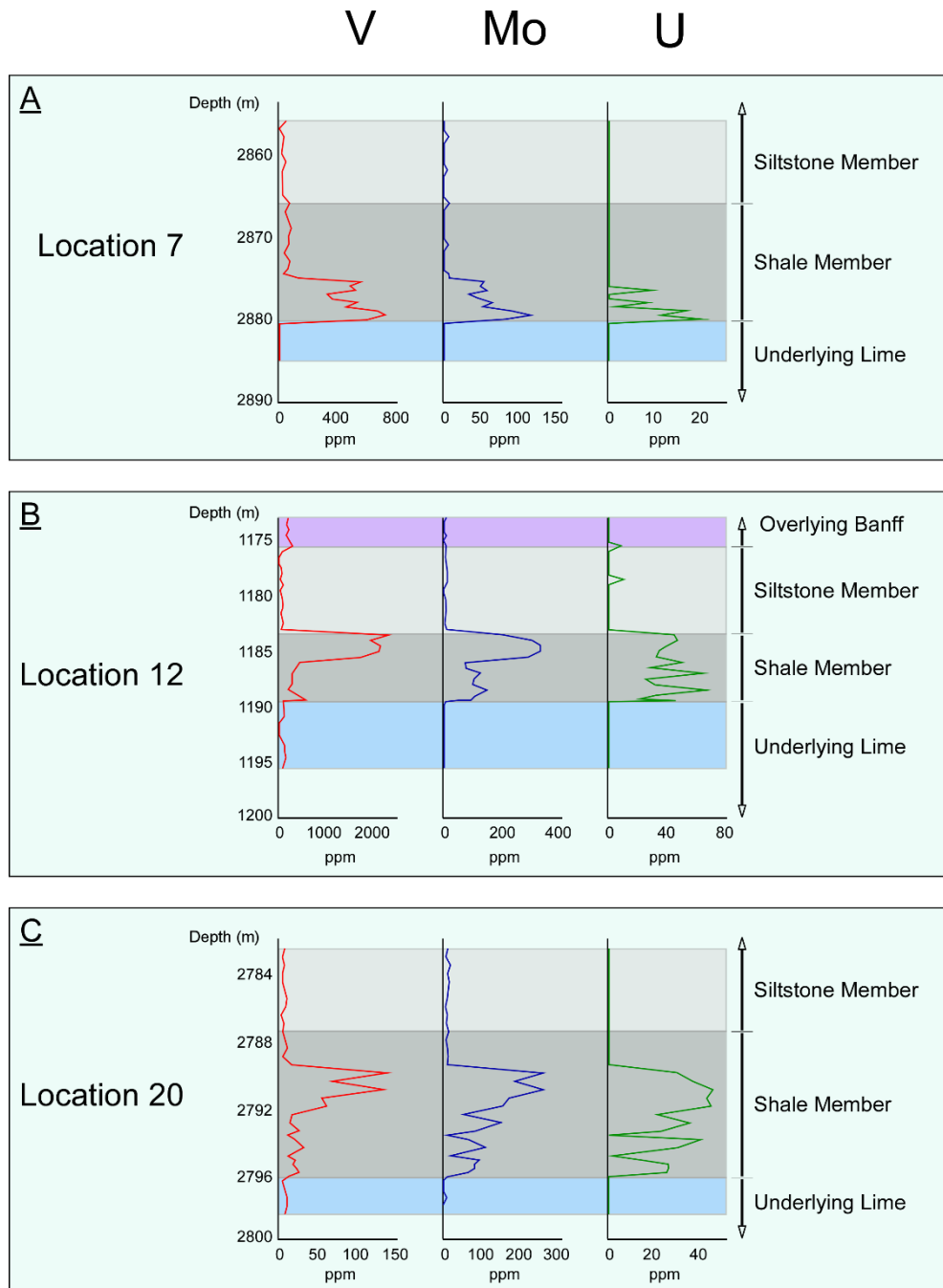


Figure 4. Exshaw Shale Formation elemental profiles of 3 redox-sensitive trace metals for locations with differing stratigraphic enrichment patterns. Elemental concentrations on the X-axes are on different scales between locations. Depths (y-axis) within colored member zones are described.

To assess the chemical homogeneity of trace metal enrichment for the Exshaw Shale Member across the region, abundances of several elements of interest are presented for the entire suite of shale member samples in the form of box and whisker plots in Figure 5. These represent the entire dataset of XRF measurements from the Exshaw Shale Member at every location (n=265). Aluminum, silicon, and calcium abundance (representing clay, silt and clay, and carbonate sediment, respectively) varies greatly in our dataset and indicates lithologic variability. The first quartile of our samples has less than 2.1% aluminum (Q1) and the fourth quartile greater than 5.8% (Q3). Nine samples have greater than 30.0% calcium and the inter-Quartile Range (IQR) has a wide span of 1.5 to 10.5% that most likely reflects variability in CaCO₃ content. The IQRs for sulfur, iron and phosphorous are all relatively narrow but with some very high outlier values. Minor elements reflect varying degrees of enrichment, with vanadium and molybdenum differing as much as an order of magnitude within their IQRs. Copper was detected in only 19% of samples with 6 samples having greater than 50 ppm and the remainder evenly distributed between 5-50 ppm. Fifty percent of samples had greater than 210 ppm with maximum values above 2000 ppm (6 samples >2000 ppm, maximum 2632 ppm). Nickel's IQR spans 60-160 ppm with a non-outlier maximum of 317 ppm and an outlier maximum of 1.1 wt.%. Molybdenum is between 8-86 ppm in 50% of samples and between 86-192 ppm for 25%. The highest observed concentration of uranium was 73 ppm and 25% of samples had greater than 17 ppm.

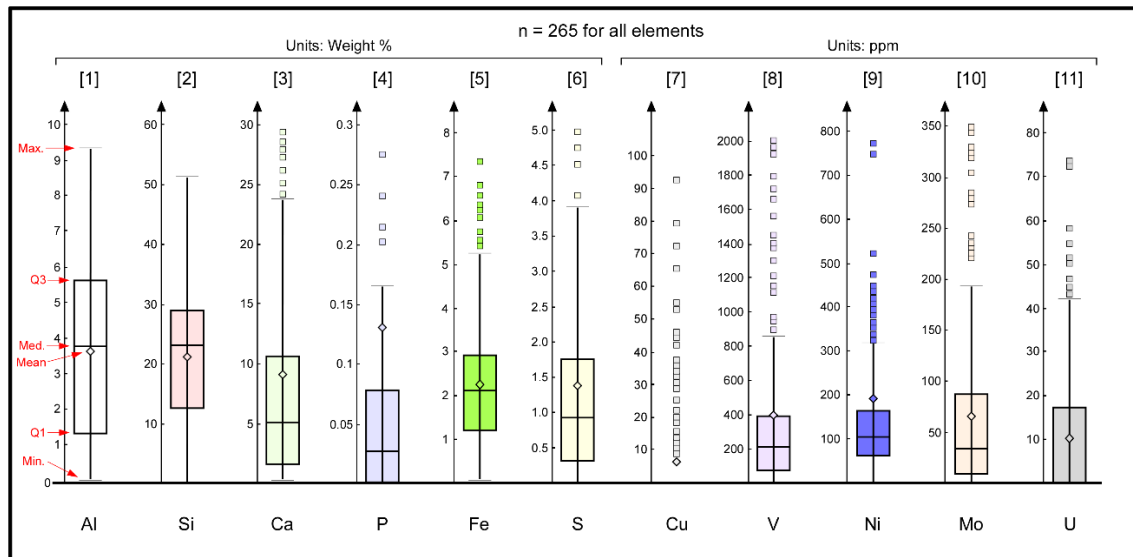


Figure 5. Box and whisker plots displaying the first quartile, median, mean, third quartile, and the minimum and maximum value that are not considered outliers (defined below). The data displayed for each element is a compilation of all 265 handheld XRF readings within the shale member for all locations studied across the basin.

The maximum and minimum (i.e., the “whiskers”) are the highest and lowest value that are not outliers.

“Outliers” are defined with the standard practice definition: a value greater than the 3rd Quartile by 1.5 *IQR or lower than the 1st Quartile by 1.5*IQR.

$$\text{IQR} = \text{Q3} - \text{Q1}$$

Outlier > $\text{Q3} + (1.5 * \text{IQR})$ or Outlier < $\text{Q1} - (1.5 * \text{IQR})$

Outliers within the chosen vertical scale appear as squares, outliers beyond the displayed vertical scale for each element are... Al: No outliers, Si: No outliers, Ca: 9 samples between 30-35.76 wt.%, P: 12 samples 0.3-9.96 wt.%, Fe: 1 sample at 9.625 wt.%, S: 7 samples between 5-10.56 wt.%, Cu: All samples displayed are outliers because the majority of samples were below detection limit, V: 6 samples between 2000-2630ppm, Ni: 3 samples between 0.120-1.057 wt.%, Mo: 2 samples between 350-520ppm, U: All in view

Elemental abundance in sediment may provide valuable information on the environment of deposition by serving as proxies for the ocean chemistry conditions that concentrated them; however, trace metals of detrital provenance may lead to misinterpretations if not considered. Metals are relatively highly concentrated in continental crust, and their eroded components enrich the transported sediments (Calvert and Pedersen, 1993; Tribovillard et al., 2006; Wedepohl, 1995). To examine relationships between trace metal concentrations and terrestrial allogenic input, aluminum (which is dominantly sourced from continental aluminosilicates) is used to represent input of continental detritus (Calvert and Pedersen, 1993; Tribovillard et al., 2006). The strength

of the correlation between Al and other select elements was evaluated (Figure 6): Si, K, Ti and Cr all correlate with aluminum, whereas Mg, P, S, Ca, V, Mn, Fe, Co, Ni, Cu, Zn, As, Rb, Sr, Y, Zr, Nb, Mo, Ba, Pb, Th and U do not. Because vanadium, nickel, molybdenum and uranium do not correlate with aluminum in the overall dataset, the effects of dilution by carbonate and detrital sedimentation can be mitigated by normalizing their concentrations to aluminum concentration via enrichment factors (EF) that use aluminum in the equation.

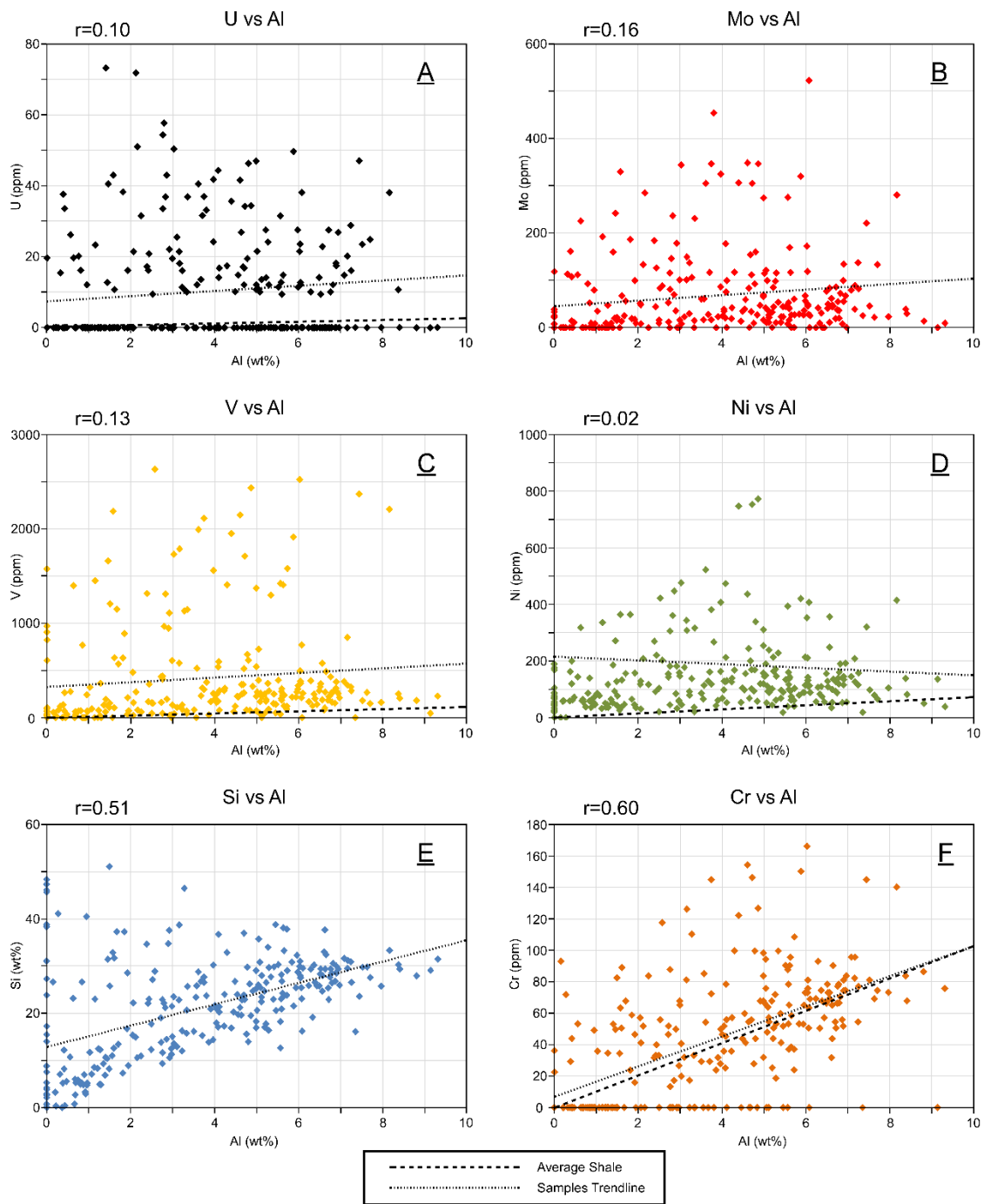


Figure 6. Cross-plots of aluminum versus elements of interest for all samples within the Exshaw Shale Member. (A): U; (B): Mo; (C): V; (D): Ni; (E): Si; (F): Cr. These plots display correlation (or not) with aluminum to predict if that element is derived from terrestrial weathering or is an authigenic precipitant. The short-dashed line is the trend line for the samples in this study. The long-dashed line is the trendline for the "Average Shale" (Wedepohl, 1971, 1995). Silicon does not have the Average Shale line because reference values are not reported for silicon in those publications. The Average Shale line for molybdenum is nearly parallel to the x-axis and thus is not displayed.

Among the 265 samples evaluated in this study, the primary redox-sensitive trace elements were in detectable concentrations in 215 for V, 252 for Ni, 200 for Mo, and 108 for U. Enrichment relative to average shale was common for each of these elements, with V, Ni, Mo and U having EF greater than 1 in 76%, 85%, 73% and 40% of samples, respectively (Figure 7); and EF greater than 100 in 1%, 1%, 32%, and 2%, respectively.

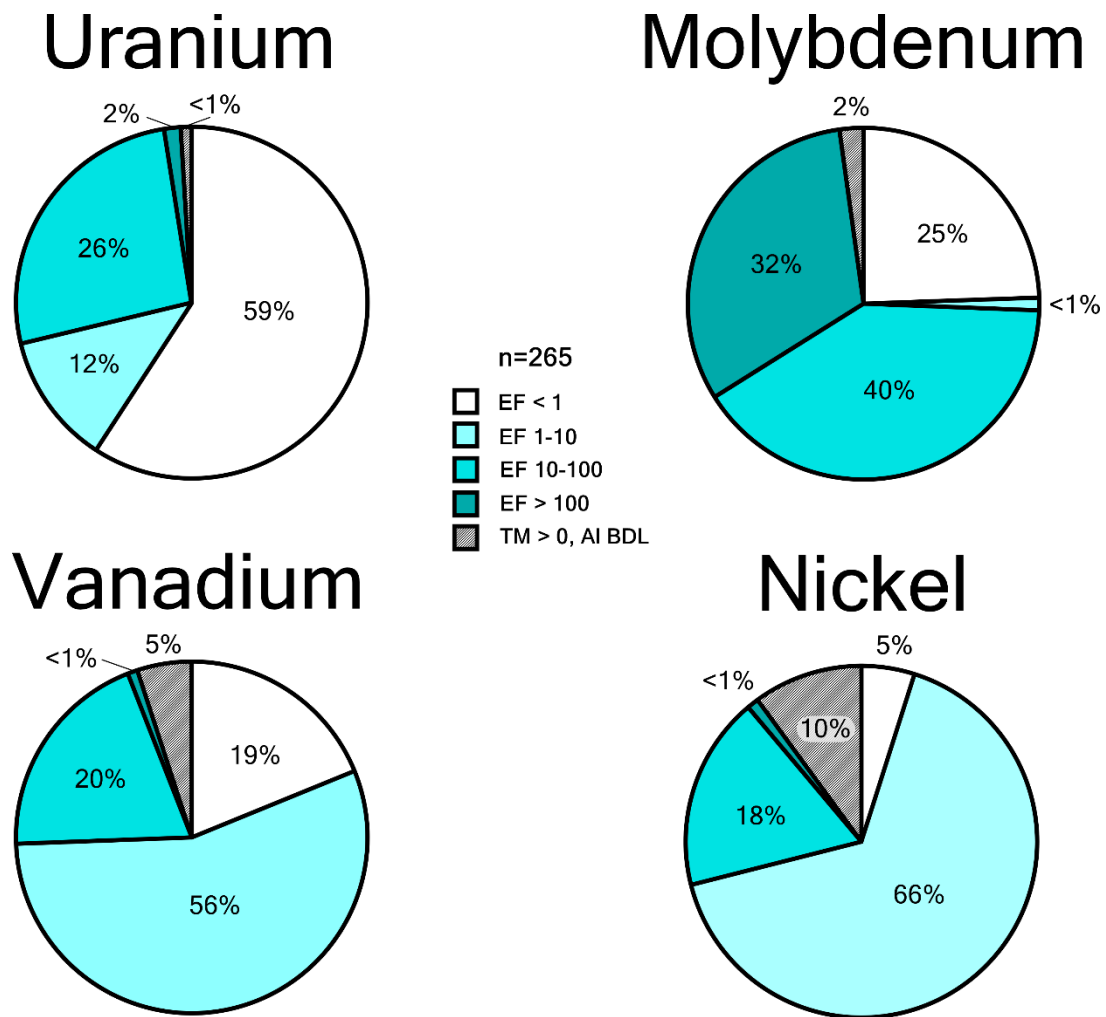


Figure 7. Redox-sensitive trace metal EF's in the Exshaw Shale Member for all samples at all locations. Each graph presents EF data in five bins: the portion of samples that (1) had the chosen trace metal in abundance less than the Average Shale (Wedepohl, 1971, 1995), (2) EF was greater than 1 and less than 10, (3) EF was greater than 10 and less than 100, (4) EF was greater than "100", (5) Aluminum was below the detection threshold but the chosen trace metal was detected (TM>0, AI BDL). The elemental concentration values used for normalization in the EF are of the Average Shale from Wedepohl (1995). Average Shale values are Al: 8.89wt.%, V: 130ppm, Ni: 68ppm, Mo: 1.3ppm, U: 3ppm.

Rock-Eval Pyrolysis

The data from Rock-Eval pyrolysis are presented in Table 2, with the corresponding elemental concentration data for each organic sample presented in Table 3. The TOC content of the Exshaw Shale Member ranges from 0.16% to 17.43% (mean = 5.45, median = 4.60) and Tmax ranges from 407 °C to 519 °C (mean = 437, median = 429). The three samples from Jura Creek did not yield valid Tmax values due to insufficient S2 to resolve peak maxima on the pyrograms, although the reported values are included in Table 2. The S1 values of samples range from 0.04 to 6.58 mg HC/g rock (mean = 1.31, median = 0.94), S2 from 0 to 95 mg HC/g rock (mean = 20.5, median = 11.4) and S3 from 0.09 to 1.54 mg CO₂/g rock (mean = 0.44, median = 0.30). The HI of samples ranges from 0 to 605 mg HC/g TOC (mean = 286, median = 340), OI from 1 to 188 mg CO₂/g TOC (mean = 16, median = 9) and PI from 0.02 to 0.83 (mean = 0.21, median = 0.10). For the sulfur-related parameters, TS ranges from 0.06% to 4.24% (mean = 1.84, median = 1.72), TOS from 0% to 3.7% (mean = 0.77, median = 0.47) and Fe-S from 0% to 3.09% (mean = 0.83, median = 0.66).

Table 2. Rock-Eval data from Exshaw Shale member organic-analysis samples

Sample	Well	Latitude	Longitude	Location #	TVD (m)	TOC (wt.%)	TS (wt.%)	TOS (wt.%)	Fe-S (wt.%)	S1	S2	S3	Tmax (°C)	HI	OI
2A	00-06-29-080-23W5-0	55.96309	-117.56459	2	1726	3.2	2.51	1.11	1.40	1.17	13.96	0.16	438	435	5
2B	00-06-29-080-23W5-0	55.96309	-117.56459	2	1728.5	17.4	1.85	1.85	0.00	4.36	95.01	0.43	432	545	2
3A	02-10-07-077-04W5-0	55.65971	-114.6061	3	702.25	4.2	3.58	0.49	3.09	1.22	22.64	0.19	407	540	7
4A	02-08-07-075-05W5-0	55.48119	-114.75242	4	1081	3.7	0.77	0.31	0.46	0.94	17.9	0.6	420	485	16
4B	02-08-07-075-05W5-0	55.48119	-114.75242	4	1084	4.6	1.06	0.44	0.62	0.9	23.22	0.66	421	504	14
5A	00-06-27-063-05W5-0	54.47699	-114.67356	5	1140.5	1.7	0.7	0.43	0.27	0.29	0.77	0.43	423	44	25
5B	00-06-27-063-05W5-0	54.47699	-114.67356	5	1146	16.6	3.7	3.70	0.00	6.58	82.66	0.34	436	499	2
6A	00-15-09-060-26W4-0	54.17836	-113.83715	6	958.5	1.6	0.09	0.00	0.00	0.25	0.8	0.51	434	50	32
6B	00-15-09-060-26W4-0	54.17836	-113.83715	6	960.5	0.7	0.12	0.07	0.04	0.07	0.13	0.16	434	20	24
7A	00-05-15-040-07W5-2	52.44017	-114.93155	7	2878.5	3.4	1.01	0.34	0.66	1.42	2.86	0.17	458	85	5
7B	00-05-15-040-07W5-2	52.44017	-114.93155	7	2880	4.6	2.63	1.00	1.61	1.6	5.04	0.14	456	110	3
8A	00-14-11-038-16W4-0	52.25597	-112.18894	8	1195.9	6.0	2.58	0.88	1.70	0.75	35.97	0.65	419	605	11
9A	00-09-32-038-10W4-0	52.3107	-111.38816	9	982	2.6	1.72	0.42	1.28	0.75	11.4	0.52	423	432	20
9B	00-09-32-038-10W4-0	52.3107	-111.38816	9	985	3.7	1.11	0.35	0.76	0.75	15.96	0.69	421	430	19
9C	00-09-32-038-10W4-0	52.3107	-111.38816	9	988	8.1	2.56	1.55	0.96	1.49	42.78	1.14	410	526	14
9D	00-09-32-038-10W4-0	52.3107	-111.38816	9	989.75	8.8	2.28	2.28	0.00	1.19	49.32	1.33	419	562	15
11A	02-08-24-027-19W4-0	51.32109	-112.54077	11	1463.5	5.8	1.31	0.46	0.84	1.25	29.57	0.61	424	508	10
11B	02-08-24-027-19W4-0	51.32109	-112.54077	11	1463.75	6.5	1.39	0.47	0.90	1.4	33.07	0.59	422	509	9
12A	02-11-10-020-13W4-0	50.68208	-111.72632	12	1185.5	7.1	2.2	0.52	1.68	1.41	32.92	1.06	417	464	15
12B	02-11-10-020-13W4-0	50.68208	-111.72632	12	1189.4	9.5	1.95	0.51	1.41	1.44	43.72	1.54	419	463	16
13A	00-07-26-016-20W4-0	50.37364	-112.64658	13	1741.6	5.4	1.4	0.88	0.52	3.01	27.94	0.25	432	521	5
13B	00-07-26-016-20W4-0	50.37364	-112.64658	13	1746.25	8.9	3.02	3.00	0.00	2.02	48.63	0.25	421	547	3
14A	00-02-15-016-27W4-0	50.34093	-113.63206	14	2703.4	7.3	4.24	0.00	0.00	0.82	6.49	0.09	460	88	1
15A	00-10-36-011-28W4-0	49.95692	-113.69304	15	3082	0.5	0.91	0.30	0.59	0.12	0.11	0.23	409	24	50
16A	00-01-28-011-24W4-0	49.93331	-113.21271	16	2228	0.2	0.63	0.18	0.44	0.17	0.13	0.30	418	81	188
17A	00-16-27-011-22W4-0	49.94557	-112.92143	17	1792.5	15.7	2.82	1.12	1.67	5.55	71.96	0.57	426	459	4
18A	00-01-12-010-26W4-0	49.80367	-113.39378	18	2533.6	1.9	0.06	0.00	0.00	1.75	5.27	0.25	446	276	13
18B	00-01-12-010-26W4-0	49.80367	-113.39378	18	2541.85	1.6	2.65	0.56	2.08	0.41	3.76	0.16	441	238	10
19A	00-01-02-006-26W4-0	49.43935	-113.39197	19	2886.45	8.2	3.85	1.73	2.10	1.75	28.64	0.2	445	349	2
20A	00-01-20-001-24W4-0	49.04564	-113.16548	20	2790	8.5	3.88	1.89	1.97	1.72	1.8	0.37	454	21	4
20B	00-01-20-001-24W4-0	49.04564	-113.16548	20	2793.75	1.0	1.12	0.00	0.00	0.38	0.51	0.09	478	49	9
20C	00-01-20-001-24W4-0	49.04564	-113.16548	20	2796	3.4	1.45	0.00	0.00	0.9	1.09	0.22	482	32	7
21A	Jura Creek	51.076548	-115.181382	21	1.57	4.8	1.55	0.71	0.82	0.05	0.01	0.16	144	0	3
21B	Jura Creek	51.076548	-115.181382	21	2.64	5.2	1.77	0.75	1.00	0.04	0.01	0.14	143	0	3
21C	Jura Creek	51.076548	-115.181382	21	5.14	4.2	2.21	0.29	1.90	0.06	0.02	0.12	142	0	3
22A	Crowsnest Pass	49.625866	-114.648981	22	4	2.7	1	0.00	0.00	0.25	1.44	0.09	483	54	3
22B	Crowsnest Pass	49.625866	-114.648981	22	9	2.4	0.31	0.00	0.00	0.08	0.74	0.81	519	31	34

Table 3. Elemental data from Exshaw Shale member organic-analysis samples. “BDL” abbreviates “below detection limit”

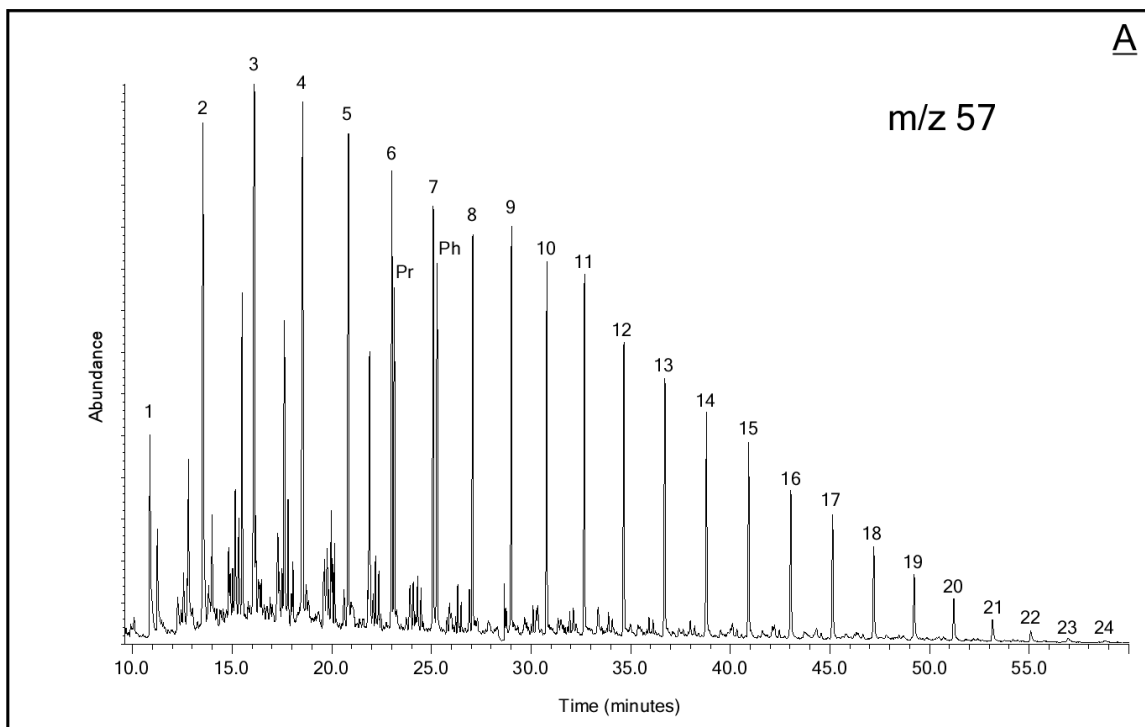
Sample	Al (wt.%)	Si (wt.%)	P (wt.%)	S (wt.%)	Ca (wt.%)	Fe (wt.%)	V (ppm)	Ni (ppm)	Cu (ppm)	Mo (ppm)	U (ppm)	V (EF)	Ni (EF)	Mo (EF)	U (EF)
2A	7.2	29.5	BDL	3.1	0.4	4.4	849	209	BDL	39	BDL	8.1	3.8	37.2	0.0
2B	6.0	31.0	0.1640	2.8	3.7	2.8	497	212	55	118	23	5.6	4.6	134.1	11.5
3A	6.6	29.4	0.0335	1.3	3.8	2.8	271	100	BDL	47	BDL	2.8	2.0	48.6	0.0
4A	4.7	23.8	0.0875	0.9	7.9	2.3	264	102	BDL	34	12	3.8	2.8	48.9	7.6
4B	4.0	20.9	0.0464	0.9	4.7	2.3	249	129	22	35	BDL	4.2	4.2	59.0	0.0
5A	2.8	9.3	BDL	0.6	22.8	1.4	47	46	BDL	BDL	BDL	1.2	2.2	0.0	0.0
5B	2.4	23.0	0.0621	3.0	1.3	3.0	352	220	79	126	21	9.9	11.8	355.1	25.3
6A	5.6	23.7	0.0964	0.1	8.4	1.5	126	62	BDL	BDL	BDL	1.5	1.4	0.0	0.0
6B	8.4	30.3	0.1347	0.5	0.5	2.5	252	139	BDL	39	11	2.1	2.2	31.8	3.8
7A	2.7	19.0	0.0760	0.9	8.3	1.4	435	155	BDL	52	BDL	10.9	7.4	131.9	0.0
7B	6.6	28.0	0.0358	1.7	2.0	2.9	575	249	BDL	83	23	6.0	5.0	86.9	10.3
8A	3.0	15.1	0.0494	2.0	1.1	5.8	133	147	65	16	BDL	3.0	6.4	36.9	0.0
9A	8.4	29.4	0.0347	0.9	2.7	3.0	205	82	BDL	30	BDL	1.7	1.3	24.1	0.0
9B	5.8	30.9	0.0376	1.2	3.8	3.0	217	80	10	28	BDL	2.5	1.8	33.1	0.0
9C	6.9	28.5	0.0234	1.6	1.0	3.4	281	135	31	134	17	2.8	2.6	133.3	7.5
9D	5.6	23.0	0.2054	2.9	5.8	3.8	202	160	80	52	13	2.5	3.8	64.2	6.8
11A	6.5	25.8	0.0376	1.3	2.9	3.6	284	156	BDL	77	14	3.0	3.1	80.8	6.4
11B	7.3	26.5	0.0363	1.2	2.8	3.5	284	158	BDL	82	16	2.7	2.8	77.3	6.6
12A	4.7	22.9	BDL	2.1	2.3	4.7	1713	754	BDL	305	34	24.8	20.9	442.4	21.5
12B	3.2	22.8	0.1532	1.1	1.4	3.4	580	344	BDL	101	21	12.6	14.3	218.8	20.2
13A	BDL	23.9	BDL	0.9	1.1	1.1	824	189	BDL	118	BDL	Al BDL	Al BDL	Al BDL	Al BDL
13B	4.7	23.6	BDL	3.2	1.6	2.9	353	201	BDL	154	17	5.2	5.6	225.3	10.9
14A	0.3	7.0	0.2406	6.6	5.6	6.4	120	2871	BDL	113	15	25.9	1188.7	2446.0	144.9
15A	0.4	0.4	BDL	0.0	33.5	0.3	BDL	63	BDL	BDL	BDL	0.0	18.7	0.0	0.0
16A	5.1	25.7	0.0722	0.9	7.3	1.8	46	52	BDL	11	BDL	0.6	1.3	14.5	0.0
17A	4.9	19.5	BDL	2.8	2.4	3.1	2436	772	BDL	346	34	34.3	20.8	487.6	21.0
18A	BDL	45.7	BDL	0.4	1.8	0.3	BDL	BDL	BDL	BDL	BDL	Al BDL	Al BDL	Al BDL	Al BDL
18B	5.1	22.5	BDL	4.7	2.3	4.0	BDL	239	BDL	11	14	0.0	6.1	14.7	7.8
19A	0.4	3.1	0.0552	0.1	19.6	0.4	41	17	BDL	17	BDL	7.8	6.2	334.0	0.0
20A	5.6	18.2	BDL	3.5	0.8	2.7	1422	393	BDL	276	32	17.5	9.2	338.8	16.8
20B	BDL	31.1	BDL	0.5	0.3	0.5	105	21	BDL	BDL	BDL	Al BDL	Al BDL	Al BDL	Al BDL
20C	6.9	29.4	0.6424	4.5	3.9	3.4	256	192	BDL	67	27	2.5	3.6	66.2	11.5
21A	4.7	37.0	BDL	0.9	0.2	1.9	519	169	BDL	112	17	7.6	4.7	162.5	10.6
21B	3.2	38.7	0.0309	0.9	0.2	2.0	1787	308	BDL	149	18	38.7	12.7	322.9	17.0
21C	5.3	27.7	0.0307	1.2	3.5	2.3	1296	228	BDL	54	BDL	16.6	5.6	68.9	0
22A	2.9	34.7	BDL	0.8	1.9	1.6	946	84	15	36	BDL	22.3	3.8	84.4	0
22B	2.6	28.9	BDL	0.7	1.9	1.5	2632	202	38	88	BDL	70.0	10.3	233.7	0

n-Alkanes and Biomarkers

The relative abundances of *n*-alkanes, hopanes, and steranes were quantified using the extracted ion chromatogram peak area (Vs) normalized to the deuterated *n*-eicosane internal standard for each sample and reported per gram TOC in the sample. Total abundances of compound classes (*n*-alkanes, hopanes, or steranes) are compared between samples as a RC, compared to the sample with the maximum concentration and calculated as:

$$\text{Relative Concentration}_{\text{Compound, Sample}} = \frac{\text{Area}_{\text{Compound, Sample}}}{\text{Area}_{\text{Compound, Max Sample}}}$$

Only peak areas from the identified compounds in this study are integrated and summed on the extracted ion chromatogram for that compound class (*m/z* 57 for *n*-alkanes, *m/z* 66 deuterated eicosane, *m/z* 191 for hopanes, and *m/z* 217 for steranes). The peaks of these compounds are displayed on chromatograms in Figure 8 and identified in Figure 9.



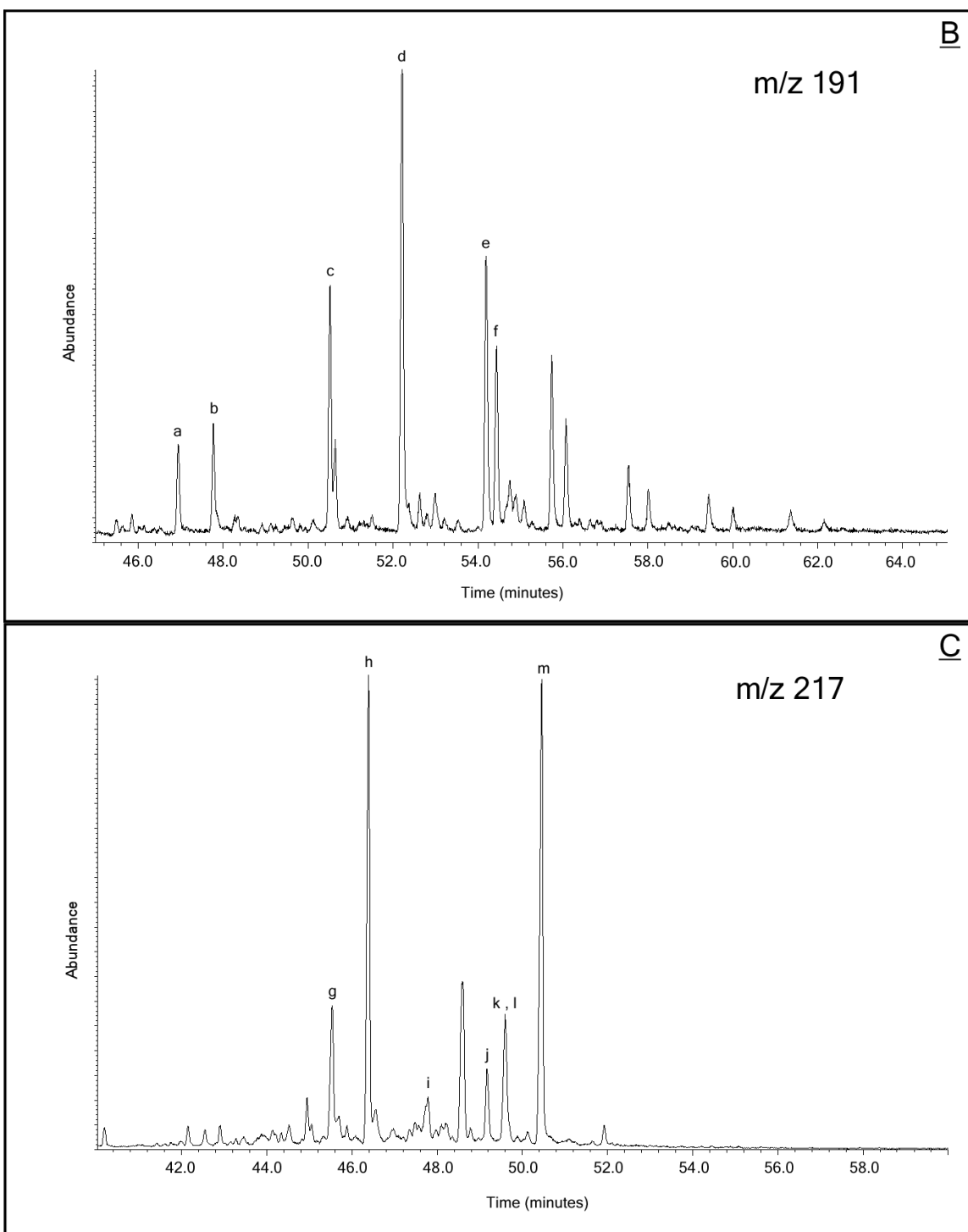


Figure 8. Extracted ion chromatograms for the three primary ions used in identification of our organic molecule suite. (a): m/z 57; (b): m/z 191; (c): m/z 217. Chromatogram A is from sample 5A, and chromatograms B and C are from sample 9D.

A m/z 57		
Peak	Compound	T _R
1	nC12	10.9
2	nC13	13.5
3	nC14	16.1
4	nC15	18.5
5	nC16	20.8
6	nC17	23.0
Pr	Pristane	23.1
7	nC18	25.1
Ph	Phytane	25.2
8	nC19	27.1
9	nC20	28.9
10	nC21	30.8
11	nC22	32.7
12	nC23	34.7
13	nC24	36.7
14	nC25	38.9
15	nC26	40.9
16	nC27	43.0
17	nC28	45.1
18	nC29	47.2
19	nC30	49.2
20	nC31	51.3
21	nC32	53.2
22	nC33	55.1
23	nC34	57.0
24	nC35	58.8

B m/z 191			
Peak	Compound	Abbr.	T _R
a	18 α (H)-22,29,30-trisnorneohopane	Ts	46.9
b	17 α (H)-22,29,30-Trisnorhopane	Tm	47.8
c	17 α (H),21 β (H)-30-norhopane	Nor	50.5
d	17 α (H),21 β (H)-hopane	Hop	52.2
e	17 α (H),21 β (H)-22R-homohopane	RHom	54.2
f	17 α (H),21 β (H)-22S-homohopane	SHom	54.4

C m/z 217			
Peak	Compound	Abbr.	T _R
g	$\alpha\beta\beta$ 20R-cholestane	BRcho	45.7
h	$\alpha\alpha\alpha$ 20R-cholestane	aRcho	46.3
i	$\alpha\beta\beta$ 20R 24S-methylcholestane	Bmet	47.8
j	$\alpha\alpha\alpha$ 20R 24S-ethylcholestane	aSeth	49.18
k	$\alpha\beta\beta$ 20R 24R-ethylcholestane	BReth	49.55
l	$\alpha\beta\beta$ 20R 24S-ethylcholestane	BSeth	49.65
m	$\alpha\alpha\alpha$ 20R 24R-ethylcholestane	aReth	50.4

Figure 9. Identification of compounds from extracted ion chromatograms presented in Figure 8 (a): m/z 57; (b): m/z 191; (c): m/z 217. Peaks on Figure 8 chromatograms are identified on the corresponding subtable in Figure 9 (A with A, B with B, C with C).

Normalized compound peak areas are used to interpret thermal maturity, OM source or depositional redox conditions via proxy ratios that compare their abundances relative to other compounds within the sample. The proxies used in this study include Carbon Preference Index (CPI from Bray and Evans, 1961), Improved Odd-Even Predominance (OEP from Scalan and Smith, 1970), Terrigenous-Aquatic Ratio (TAR

from Bourbonniere and Meyers, 1996), %Ts, Ts/Hop, %22S, Nor/Hop, %20S and % $\alpha\beta\beta$. Equations for each are presented below, compound identification and abbreviations are provided in Figure 9, and ratio values for OM samples are presented in Table 4. CPI and OEP measure the predominance of odd carbon number n-alkanes compounds relative to even-numbered n-alkanes to determine the biological source of OM. TAR measures the predominance of long-chain n-alkanes over short-chain n-alkanes to determine biological source of OM. %Ts measures the abundance of the more thermally stable Ts over Tm to assess thermal maturity. Ts/Hop measures the abundance of Ts over C₃₀ hopane to assess thermal maturity. %22S measures the abundance of the S isomer over the R isomer of C₃₁ homohopane to assess thermal maturity. Nor/Hop suggests an anoxic carbonate depositional environment for samples that have C₂₉ norhopane in greater abundance than C₃₀ hopane. %20S and % $\alpha\beta\beta$ measure relative abundances of S over R isomers and $\alpha\beta\beta$ over $\alpha\alpha\alpha$ isomers in C₂₉ ethylcholestane respectively to assess thermal maturity (Peters et al., 2005b). Equations for each ratio are as follows:

$$CPI = \frac{2(nC23 + nC25 + nC27 + nC29)}{nC22 + 2(nC24 + nC26 + nC28) + nC30}$$

$$OEP = \frac{nC21 + 6(nC23) + nC25}{4(nC22 + nC24)}$$

$$TAR = \frac{nC27 + nC29 + nC31}{nC15 + nC17 + nC19}$$

$$\%Ts = \frac{Ts}{Ts + Tm}$$

$$Ts/Hop = \frac{Ts}{Hop}$$

$$\%22S = \frac{SHom}{SHom + RHom}$$

$$Nor/Hop = \frac{Nor}{Hop}$$

$$\%20S = \frac{\alpha Seth}{\alpha Seth + \alpha Reth}$$

$$\% \alpha \beta \beta = \frac{\beta Reth + \beta Seth}{(\beta Reth + \beta Seth) + (\alpha Reth + \alpha Seth)}$$

Table 4. Organic molecular data ratios from Exshaw Shale Member organic-analysis samples. Samples that do not report a value for a ratio did not detect either of the compounds involved. “#/0” indicates that a value existed only in the numerator, “0/#” indicates that a value existed only in the denominator.

Sample	Pr/Ph	TAR	OEP (C ₂₁ -C ₂₅)	CPI	Ts/Hop	%Ts	%22S	%20S	% $\alpha\beta\beta$	Nor/Hop	n-Alkane (RC)	Hopanes (RC)	Steranes (RC)
2A	0.96	0.11	0.95	1.07	0.17	0.30	0.62	0.47	0.56	0.38	0.20	0.19	0.30
2B	1.11	0.00	0.91		0.19	0.22	0.63	0.72	0.50	0.00	0.01	0.03	0.04
3A	0.60	0.11	0.90	0.91	0.09	0.17	0.51	0.16	0.23	0.32	0.07	0.14	0.95
4A	0.86	0.15	0.91	1.15	0.13	0.29	0.42	0.11	0.24	0.33	0.09	0.06	0.25
4B	0.78	0.02	1.10	1.34	0.21	0.29	0.42	0.15	0.24	0.46	0.05	0.10	0.60
5A	0.80	0.24	0.95	1.01	0.19	0.47	0.61	0.47	0.53	0.46	0.40	0.32	0.28
5B	0.86	0.06	0.99	1.07	0.24	0.32	0.60	0.62	0.53	0.62	0.03	0.06	0.10
6A	1.27	0.01	0.84	1.43	0/#	0/#		0.23	0.22	0/#	0.19	0.04	0.05
6B	2.23	0.00	0.90	3.14	0/#					0/#	0.51	0.01	0.00
7A	1.11	0.05	0.92	1.19							0.22	0.00	0.00
7B	1.36	0.04	0.97	1.08	0/#			0/#	0.27	0/#	0.25	0.01	0.03
8A	0.86	0.04	1.01	0.91	0.07	0.18	0.49	0.13	0.22	0.36	0.07	0.23	0.99
9A	1.18	0.00	0.54		0.04	0.37	0.37	0.11	0.26	0.12	0.22	0.23	0.56
9B	1.09	0.00	0.98	1.18	0.05	0.23	0.55	0.11	0.29	0.16	0.17	0.17	0.53
9C	0.83	0.01	0.88	1.50	0.11	0.24	0.39	0.13	0.23	0.29	0.08	0.09	0.51
9D	0.82	0.11	0.99	1.00	0.13	0.21	0.46	0.13	0.22	0.39	0.06	0.17	0.80
11A	1.36	0.12	1.01	1.33	0.10	0.31	0.58	0.18	0.23	0.26	0.08	0.13	0.60
11B	1.38	0.13	1.03	1.23	0.17	0.32	0.59	0.19	0.25	0.31	0.07	0.11	0.60
12A	1.65	0.01	1.00	1.02	0.11	0.23	0.40	0.16	0.30	0.19	0.05	0.01	0.07
12B	1.49	0.00	0.86	0.91	0/#	0/#		0/#	0.28	0/#	0.02	0.01	0.09
13A	1.11	0.15	0.96	0.82	0.20	0.28	0.62	0.48	0.48	0.49	0.15	0.12	0.63
13B	1.10	0.01	0.99	1.09	0.11	0.21	0.59	0.46	0.43	0.43	0.02	0.05	0.16
14A	1.44	0.01	1.13	1.16							0.00	0.00	0.00
15A	1.38	0.01	0.88	2.32							0.31	0.00	0.00
16A	1.72	0.00	1.42		0/#					0/#	0.27	0.10	0.00
17A	1.45	0.06	0.98	1.03	0.15	0.18	0.59	0.43	0.26	0.42	0.04	0.02	0.21
18A	NA	NA	NA	NA	NA	NA	NA	NA	NA	NA	NA	NA	NA
18B	1.12	0.02	0.98	1.12	0.22	0.51	#/0	0.37	0.44	0.39	0.28	0.07	0.14
19A	1.32	0.01	0.98	1.07	0.44	0.71	#/0	0.32	0.42	0.27	0.06	0.01	0.02
20A	1.11	0.11	1.00	0.92	0/#			0/#	0/#	0/#	0.06	0.00	0.00
20B	0.63	0.51	0.96	0.96	0.29	0.42	0.57	0.45	0.50	1.09	1.00	1.00	1.00
20C	1.74	0.00	1.00	1.12							0.07		
21A	NA	NA	NA	NA	NA	NA	NA	NA	NA	NA	NA	NA	NA
21B	NA	NA	NA	NA	NA	NA	NA	NA	NA	NA	NA	NA	NA
21C	NA	NA	NA	NA	NA	NA	NA	NA	NA	NA	NA	NA	NA
22A	1.40	0.02	0.91	1.28	0/#			0/#	0.43	0/#	0.03	0.00	0.01
22B	1.41	0.09	1.00	1.34	0.06	0.43		0/#	0/#	0.23	0.11	0.01	0.01

Sample 20B has the greatest total peak area for all three compound classes, making it the reference point for comparison of RCs ($RC_{20B} = 1.00$ for all three classes). After 20B, samples 2A, 5A, 6B, 7A, 7B, 9A, 15A, 16A, and 18B have the highest n-alkane concentration ($RC_{alkanes} = 0.20$ to 0.51) and are not associated with low Tmax, high TOC, or a trend in OEP, TAR or CPI. High abundances of hopanes and steranes occur within samples 2A, 3A, 5A, 8A, 9A, 9B, 9D, 11A, 11B and 13A ($RC_{hopanes} = 0.11$ - 0.32 , $RC_{steranes} = 0.28$ - 0.99), and all of these samples have low to moderate Tmax values

(Tmax = 407-438 °C). Steranes were detected in 27 of 37 analyzed samples and hopanes were detected in 30 samples. Several of the samples that have relatively high steranes ($RC_{steranes} > 0.25$) and hopanes ($RC_{hopanes} > 0.1$) have relatively low n-alkanes ($RC_{alkanes} < 0.1$). Homohopane peaks of chain-length C₃₂ and beyond (paired-peaks displayed on chromatogram B of Figure 8 beyond peak “f”) were resolvable in very few samples but were most often small and obscure, so although they are observed in the Exshaw Shale Member, they are not prominent or consistent enough across locations to be investigated in this study. For the m/z 57 ratios, Pr/Ph ranges from 0.60 to 2.23 (mean = 1.20, median = 1.12), TAR from 0 to 0.51 (mean = 0.07, median = 0.02), OEP from 0.54 to 1.42 (mean = 0.96, median = 0.98), and CPI from 0.82 to 3.14 (mean = 1.22, median = 1.10). For hopane ratios, Ts/Hop ranges from 0.04 to 0.44 (mean = 0.16, median = 0.16), %Ts from 0.17 to 0.71 (mean = 0.31, median = 0.29), %22S from 0.37 to 0.63 (mean = 0.53, median = 0.57), and Nor/Hop from 0 to 1.09 (mean = 0.36, median = 0.34). For sterane ratios, the %20S ratios range from 11% to 72% (mean = 30%, median = 21%), and % $\alpha\beta\beta$ ranges from 22% to 56% (mean = 0.34%, median = 0.28%).

CHAPTER FOUR

Discussion

Stratigraphy

Within the core included in this study, the Exshaw Shale Member is slightly thicker on average than reported in previous studies (Caplan, 1997; Peters et al., 2005b). The Exshaw Shale Member was less than 3 m thick at three locations, and greater than 8 m thick at seven (mean = 5.67 m, median = 4.1 m). Observations of differing thickness are consistent with previous studies that report variable thicknesses for each member, including parts of the central region of Alberta that have a thin Exshaw Shale Member and no Siltstone Member (Caplan, 1997; Rokosh et al., 2012). The Siltstone Member was often highly calcareous ((Macqueen and Sandberg, 1970; Robison, 1995) and confusingly appears similar to Banff carbonates through central Alberta (Caplan, 1997; Rokosh et al., 2012). The similarity between the Exshaw Shale and Banff Formation regarding physical appearance, thickness, and organic richness (Macqueen and Sandberg, 1970) makes differentiation of these units difficult, particularly when differentiation is exclusively reliant upon well log response.

Stratigraphic trace element enrichment patterns within the Exshaw Shale Member differ across the basin (Figure 4). The most common case is to exhibit enrichment but have no prominent pattern through the shale (locations 3, 4, 15, 16, 18 and 22). Multiple locations either decrease (locations 7, 9, 11 and 21) or increase (locations 6, 12, 13 and 20) upward. Location 2 is most enriched in the middle of the member, and location 5 is

most enriched near the upper and lower contacts. The Exshaw Shale Member was too thin at the remaining sites (locations 8, 14, 17 and 19) to observe a stratigraphic enrichment pattern. These results expand on previous studies that report upward increasing trace metal enrichment for two cores (Caplan and Bustin, 1996, 1998). The wells in these studies are located in the Peace River Embayment near location 2 in the present study where maximum trace metal enrichment was detected within the middle portion of the Exshaw Shale Member, although the sampling resolution was lower and may not have captured the corresponding enrichment trend. The upward decreasing enrichment pattern is prevalent in the central locations on the paleogeographic shelf (Figure 1). A cluster of sites in the south (locations 14, 15, 16, 17, 18 and 19) with no prominent enrichment pattern or relatively thin shale intervals are near the edge of the contemporaneous Madison Shelf proposed by Richards (1989) where bathymetric relief over short distances can result in significant changes in redox conditions. The lack of a basin-wide trend in enrichment patterns suggests that trace metal sequestration across the study area is more strongly influenced by local factors than a dominant basin-wide ocean-chemistry condition.

Depositional Environment

Marine Shelf to Shelf Slope

The relative proportion of major constituent elements, calcium from carbonate minerals, aluminum from clay, and silica from silt and clay, varies greatly within cored intervals and across the WCSB. This may suggest that the sources of clastic sediment were not consistent and that either detrital minerals were being variably contributed, or

that locally high amounts of biogenic silica or carbonate minerals diluted a regionally consistent clay component at some locations. Given the high IQRs of silicon and calcium (Figure 5), the latter scenario seems most likely. Aluminum has a large IQR, with the median (4.23%) and mean (4.07%) well below the Average Shale value of 8.89% (Wedepohl, 1995). This suggests that clay abundance in the Exshaw Shale Member is lower and less consistent across the basin than indicated by previous literature (Caplan and Bustin (1996) mean 9.57%; Caplan and Bustin (1998) mean 7.0%). Silicon correlates well with aluminum ($r=0.75$, Figure 6); however, high proportions of biogenic silica are not observed in any previous studies, so changes in the amount of silica were likely affected by variations in the silicate proportion of allocthenic detritus. Silica's first quartile and median values ($Q_1=12.5\%$, median= 23.0% , Figure 5) are sufficiently high to suggest a common detrital silt component across most sites in addition to the silicon present in clay minerals. This is consistent with core observations in this study and others (Caplan and Bustin, 1996, 1998) that identify silt-sized grains and alternating laminations of clay and silt. Several samples are completely void of silicon and several are near the theoretical maximum (46.7%) and indicates that the Exshaw Shale Member can host both silt-rich and silt-free lithologies.

A negative correlation exists between aluminum and calcium ($r=0.65$) and the amount of calcium varies greatly, with some samples having less than 1% and others having greater than 20%. Several samples from the Exshaw Shale Member have sufficient calcium abundance to be classified as limestone and greater than half of the specimens were at least mildly calcareous (Ca median $\sim 5\%$). This is supported by the qualitative observation during core description that the majority of Exshaw Shale

Member specimens observed across locations were reactive to 10% HCl. Previous literature concludes that transgression and enhanced upwelling during Exshaw Shale Member deposition terminated platform carbonate production due to eutrophication (Caplan and Bustin, 1996, 1998, 2001). Thus, the widespread presence of calcite may be detrital carbonate sediment derived from shelf erosion rather than autochthonous, in situ marine carbonate sediment production and accumulation. Echinoderm (crinoid) skeletal fragments were observed in every core either within the Exshaw Shale Member or conformably overlying strata. This suggests the production of marine allochems in shallow water and subsequent transport into deeper, anoxic environments.

Redox Conditions

Sediment deposited under suboxic or anoxic bottom waters (reducing or strongly reducing conditions, respectively) will often exhibit enrichment of redox-sensitive trace metals (Arthur and Sageman, 1994; Calvert and Pedersen, 1993; Tribovillard et al., 2006; Vine and Tourtelot, 1970). Two major factors that can limit the amount of enrichment include: (1) dilution from high influx of terrestrial sediment, biogenic silica, and carbonate minerals or (2) low availability of dissolved trace metals due to either a stratified water column that prevents mixing or a restricted basin with minimal influx of water from the open ocean (Algeo et al., 2007; Algeo and Rowe, 2012; Brumsack, 2006; Liu and Algeo, 2020; Tribovillard et al., 2006). EFs help correct for differences in carbonate or detrital sediment content in samples through normalization to aluminum. Phosphorous, iron, sulfur, vanadium, nickel, molybdenum and uranium are not correlated to aluminum (Figure 6), so variable concentrations in those elements can be attributed to oceanographic controls rather than provenance of sediment (Tribovillard et al., 2006).

V, Ni, Mo, and U Enrichment Factors. Molybdenum is highly enriched in a large portion of samples (32% of samples have EF > 100), and the majority are enriched beyond EF 10 (Figure 7). The high levels of molybdenum enrichment imply suboxic or anoxic reducing conditions for three quarters of our samples (Tribovillard et al., 2006). Vanadium and nickel have similar enrichment patterns and are moderately enriched (EF 1-10) for the majority of samples. Uranium is enriched in 40% of Exshaw Shale Member samples, but not to the extent of the hyper enrichment expected under euxinic conditions (Brumsack, 2006; Tribovillard et al., 2006). These observations suggest that the basin experienced reducing bottom water conditions at least occasionally to preserve these relatively high concentrations of redox-sensitive trace elements. However, they also suggest that there was not consistently anoxic or euxinic conditions across the entire basin because those settings would cause even higher enrichment factors across even more samples, especially for uranium and vanadium (Tribovillard et al., 2006). Redox extremes on either end of the spectrum are unlikely; neither basin-wide euxinia nor basin-wide oxygenation existed throughout accumulation. This level of enrichment for V, Ni, Mo, and U may be explained by either intermittent periods of oxygenation in a regularly anoxic basin, or consistent but less intense maintained oxygen-limitation. Overall, all redox-sensitive elements are over 10 times as enriched as the Average Shale in at least 20% of the samples and at least 73% of samples are more enriched than the Average Shale for all elements except uranium (Figure 7). Aluminum is less than half as abundant as the Average Shale in more than 50% the samples (median Al = 4.23 wt.% versus 8.89 wt.%). This contributes greatly to EF when trace metals are present and appropriately

represents allogenic enrichment, because lower aluminum likely coincides with fewer redox-sensitive trace metals when ocean chemistry is held constant.

Ni/Co, V/Mo, V/Ni, V/Cr Ratios. Vanadium and nickel are both enriched for 76% of samples, and proxy ratios involving each of these elements can be used to more confidently identify depositional redox conditions in many scenarios (Baioumy and Lehmann, 2017; Hatch and Leventhal, 1992; Liu and Algeo, 2020; Rimmer, 2004). For our interpretations, we consider the suggested value ranges for oxygen availability used by Baioumy and Lehmann (2017) and references therein (Table 5). The Ni/Co ratio estimates that 68% of the samples were deposited under anoxic conditions. Of these, some exceed the “anoxic” threshold by a small margin (ten samples Ni/Co = 7 to 10) and some exceed it greatly (fifteen samples Ni/Co = 10 to 115) with no geographic grouping for high or low values. V/Mo suggests that most of those same samples are suboxic rather than anoxic, and only gives an anoxic designation to one single sample.

Table 5. Redox-sensitive trace metal ratio proxies and their value cutoffs from Baioumy and Lehmann (2017) and references therein

Ratio	Oxic	Suboxic	Anoxic	Sample Mean	# of non-zero samples
Ni/Co	<5	5-7	>7	18.6	27
V/Mo	10-60	2-10	<2	8.0	31
V/Ni	<1.9	1.9-3.0	>3.0	3.0	34
V/Cr	<2.25	2.25-4.5	>4.5	8.1	28
Th/U	7		2	0.6	19

Although ratios may not agree on the degree of oxygen limitation, spatial trends are evident when location values are observed relative to other locations for each ratio. Locations 2, 3 and 4 in the north all suggest greater oxygen depletion for each ratio, and

samples from locations 5 and 6 either have values that trend toward greater oxygenation or have undetectable trace metals, which also suggests oxidizing conditions. Location 7 in central Alberta appears more oxygen-limited, whereas locations 8 and 9, despite being in close proximity, contrast strongly as location 8 has the strongest signal for oxygenation and location 9 has evidence for low oxygen conditions in all samples. Location 11 ratios suggest oxygenation, and the locations farther south have variable levels of anoxia (locations 12, 14, 15, 16, 18). Some of the locations in or on the margin of the Prophet Trough (Figure 1) exhibit strong and consistent anoxic values (locations 17, 19, 20, 21, and 22). The anoxia proxies for the outcrops (locations 21 and 22) all suggest anoxia except for V/Mo, which suggests oxygenated conditions for 4 out of 5 outcrop samples. V/Ni suggests the greatest diversity of any ratio; the samples are equally divided between oxygenation categories. V/Cr considers all samples with chromium to be suboxic (ten samples) or anoxic (seventeen samples) except for location 8, which is also the only oxic location suggested by Ni/Co. The Th/U ratio for every sample with uranium is well below the threshold for anoxia ($\text{Th/U} = 0.2$ to 1.6). However, with twelve samples having detectable levels of thorium and undetectable levels of uranium, it is likely that several of these samples would yield higher Th/U values if the low concentrations of uranium were quantifiable. Redox-sensitive trace metal ratios suggest more oxygen limited conditions in the Peace River Embayment and Prophet Trough than on the adjacent shelf, and the locations near the shelf edge in the south exhibit the most disagreement between proxies. Combining input from all 5 ratios, the data suggests that all locations experienced some degree of oxygen limitation with the paleogeographic high regions (Rundle and Madison

Shelves) experiencing suboxic conditions and the low regions (Peace River Embayment and Prophet Trough) experiencing strongly suboxic/anoxic conditions.

Phosphorous. The phosphorous concentration in most samples was very low relative to the Average Shale (median 0.027% versus 0.070%; Figure 5) and phosphate nodules were not commonly identified in core though they were observed at the Crowsnest Pass and Jura Creek outcrops as up to several centimeters in diameter. This could be indicative of higher phosphorous precipitation in the deeper water regions of the basin and their correspondingly more strongly reducing conditions. The occurrence of phosphate nodules may explain several exceptionally high concentration outliers in core samples. XRF sampling likely included some measurements from phosphate nodules. Some of these phosphate-bearing cores also have high sulfur concentration outliers that may reflect areas of concentrated pyrite (FeS_2). Highly concentrated sedimentary phosphorous can accompany upwelling and OM preservation (Tribovillard et al., 2006), but interpretation of a particular causal mechanism for the samples analyzed in this study is difficult (Tribovillard et al., 2006).

TS vs TOC. A cross plot of TS vs TOC broadly suggests that most of our locations are close to normal oxic marine conditions with a few possibly implying anoxic conditions (Figure 10). Assessing points plotted on a TOC-Fe-TS ternary diagram, however, provides a more robust assessment of euxinia and pyritization (Figure 11; Arthur and Sageman, 1994). By considering iron, we can assess the role of pyrite in the incorporation of sulfur in sediments. Low availability of reactive iron in restricted basins can limit pyrite precipitation and therefore the sulfur content of marine sediments (Arthur

and Sageman, 1994; Dean and Arthur, 1989). If TS/Fe ratios plot along the 1.15 ratio line (stoichiometric pyrite ratio), all the reactive sulfur was reduced and precipitated as pyrite. TS/Fe ratios greater than 1.15 indicate that other forms of sulfur beyond pyrite are present (e.g., organic sulfur or sulfates) and therefore not all sulfur was reduced in pyrite. TOC on this diagram helps identify non-organic-rich rock that has concentrated pyrite not associated with organic matter deposition, such as a winnowed sandstone.

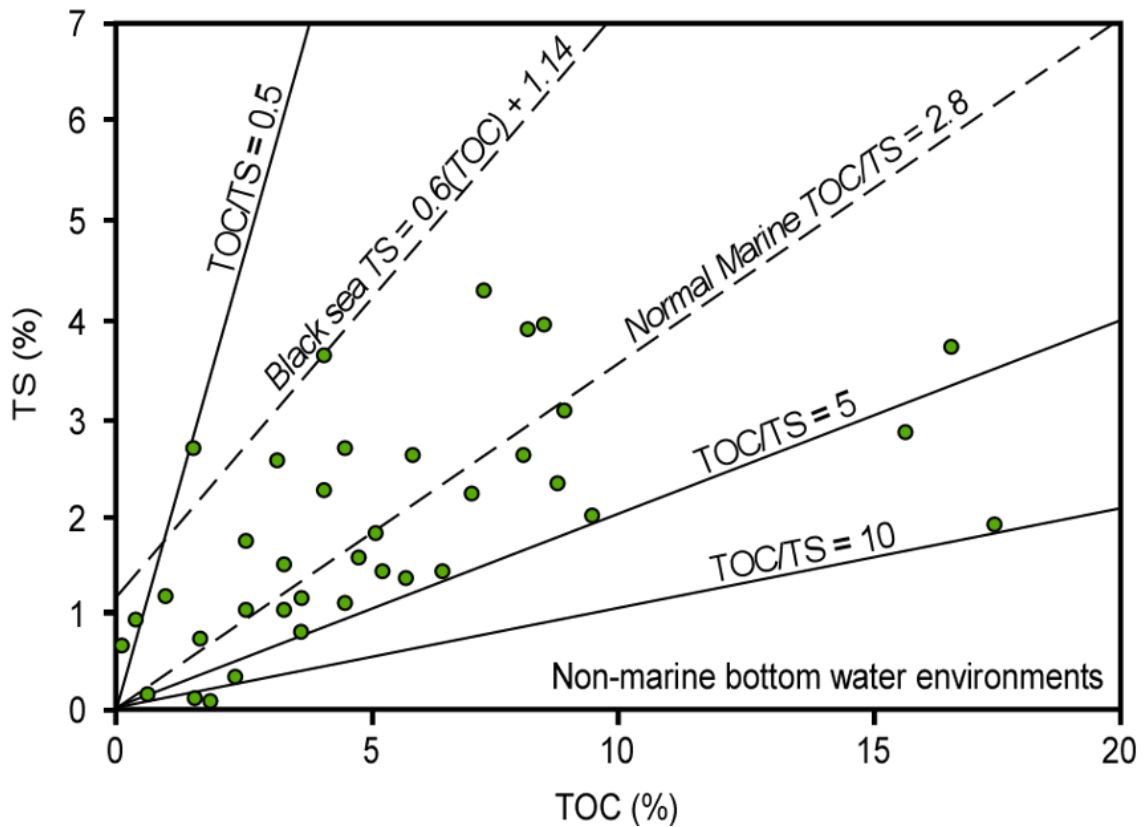


Figure 10. TS vs TOC crossplot displaying trend lines for modern marine sediments in normal marine conditions and the Black Sea. Lower TOC/TS ratios (steeper slope) are interpreted as more reducing conditions. After (Qiao et al., 2021) and references therein.

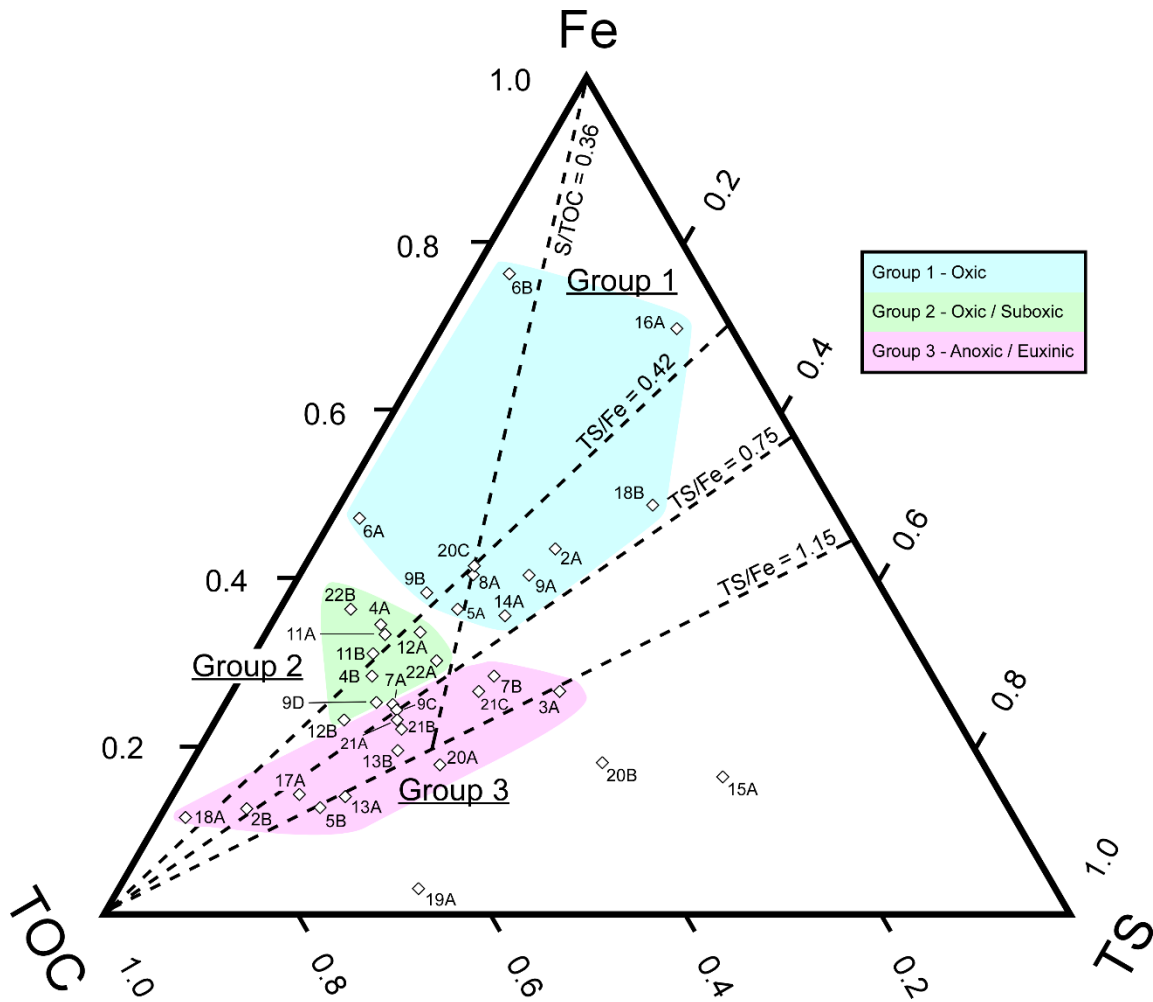


Figure 11. Ternary diagram to assess depositional conditions exclusive of the redox-sensitive trace metals U, Mo, or V. The line $S/TOC=0.36$ is the typical trend for fully oxic conditions. $TS/Fe = 1.15$ is the stoichiometric ratio of pyrite, graphically indicating that all iron was reduced and fixed in pyrite. Points plotting graphically far left or far right of the 0.36 S/C trendline indicate euxinic conditions that are organic carbon limited ($S/C > 0.36$) or iron limited ($S/C < 0.36$). S/Fe ratio trendlines of 0.42, 0.75 or 1.15 indicate suboxic, anoxic or euxinic conditions, respectively (Arthur and Sageman, 1994; Dean and Arthur, 1989; Liu and Algeo, 2020).

Our samples typically fall into three primary groupings on Figure 11: oxic (group 1), oxic/suboxic (group 2), and anoxic/euxinic (group 3). Based on both elemental and Rock-Eval chemistry, samples 13A, 14B, 15A, 18B, and 19A are also determined to be oxic. Sample 20B is high in silicon with no detected aluminum and indicates a quartzose lithology. The rock is black in color with no visible pyrite and no Fe-S (pyrite) from Rock-Eval. Accordingly, this sample is likely anoxic/euxinic and is excluded from group

3 due to the lithologic differences. Samples 21A, 21B, 21C, 22A and 22B all plot as possibly suboxic or euxinic suggesting that the Prophet Trough was less oxygenated than the shallow shelf to the northeast of locations 21 and 22 (Figure 1; Richards, 1989). The locations clustered in southern Alberta have disagreement between sites. This supports the hypothesis that these locations are close to the shelf edge where local bathymetry (within 10's of kilometers) would have great influence on the depositional conditions, i.e., areas prone to periodic sediment-gravity flows and associated bottom-water ventilation.

Because the study area includes locations across a wide range of thermal maturity, interpretations must consider the possibility of carbon and sulfur loss from hydrocarbon expulsion. For samples subjected to high thermal maturity, a decrease in organic carbon and organic sulfur and static iron concentration is likely, and results in an upward migration of points on the TOC-Fe-TS ternary diagram. This issue does not appear to be the circumstance for this dataset, as indicated by mature (7A, 7B, 20A, 20B) and overmature (21A, 21B, 21C) samples plotting within the graphically low euxinia bounds. Locations 2, 5, 9, 18 and 20 each have samples that plot in different groups as a result of stratigraphic variability. Variations between samples from the same location may be explained by alternations in oxygen availability reflected in the vertical profile. Oxygen, however, can penetrate several centimeters below the sediment/water interface and oxidize elements that accumulated during reducing conditions (Tribovillard et al., 2006), thus complicating the preservation of vertical changes.

Organic Matter Source

Sedimentary OM derived from marine algae has predominantly short-chain n-alkanes (<nC₂₅) whereas OM from higher plants has an increased proportion of long-chain alkanes (Peters et al., 2005a, b). (Robison, 1995) observes an abundance of short-chain alkanes in Exshaw extracts from 15 cored wells. This study also observes short-chain alkanes basin-wide and suggests that OM is dominantly marine in origin. The n-alkane distributions across the basin do not show an odd-chain-number preference whether measured by CPI or OEP, suggesting a lack of thermally immature organic matter from terrestrial sources (Figure 12). Locations to the northeast are the most likely to have terrestrial sources because of their proximity to the contemporaneous continental landmass (Richards et al., 1994; Witzke, 1990), but only two samples from the northeast (6B and 9C) have odd-carbon preferences; all others suggest marine sources and/or thermal maturity. TAR are low for all samples as well (Table 4), further confirming marine plankton as the dominant organic matter source for the Exshaw Shale. Copper is in low concentration basin-wide, and although this element can be enriched in sediments deposited in upwelling zones (Calvert and Pedersen, 1993), the presence (or absence) of Cu is complicated by its mobility in sediment pore fluids and associated tendency to migrate away from OM-rich layers.

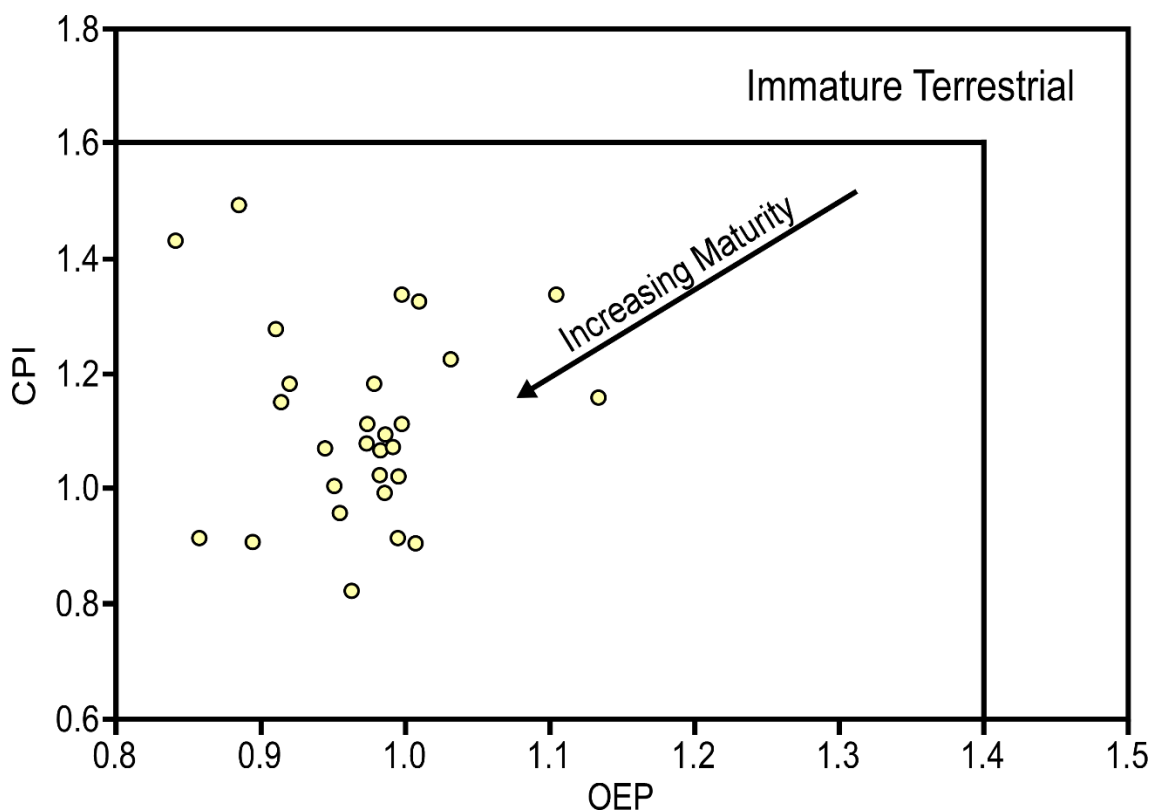


Figure 12. CPI vs OEP crossplot comparing two n-alkane ratios that each measure the dominance of odd carbon number n-alkanes in a sample. Values beyond 1.6 CPI or 1.4 OEP suggest terrestrial OM input and low thermal maturity, values below those thresholds indicate marine OM and/or thermal maturation. Both ratios decrease to an equilibrium of 1.0 with increasing thermal maturity. A value significantly below 1.0 for either ratio suggests an immature sample from hypersaline conditions (Peters et al., 2005b).

Pr/nC₁₇ vs Ph/nC₁₈

A cross plot comparing Pristane/nC₁₇ against Phytane/nC₁₈ (Figure 13) uses two ratios that are both affected by thermal maturity, OM source, and redox conditions to better isolate the likely control on variability (Peters et al., 2005b; Shanmugam, 1985). Plotted samples strongly agree with Tmax values for thermal maturity; samples with higher Tmax plot closer to the origin. Samples from the same location plot near each other and provide confidence in the ratios' consistent reaction to thermal alteration. This also implies that depositional conditions at most locations were not dramatically different during sample deposition (i.e., similar OM sources and redox conditions). The

distribution of points suggests marine plankton as the dominant organic source across the basin. An exception to this trend is location 20, which includes sample 20B that was deposited in more reducing conditions than the samples stratigraphically above and below it, and/or had an even greater proportion of planktonic organic matter. The two points on the lower boundary for higher plant OM are from the overmature location 22 that from other proxies is not predicted to have terrestrial input (i.e., low TAR, low OEP and CPI as shown in Table 4 and Figure 12). Therefore, even these samples most likely contain primarily planktonic OM. On Figure 13, locations 2, 12, 20 and 22 contain samples that suggest different thermal maturities than samples from the same location and highlight the value of considering multiple proxies for any given attribute. Biodegradation could be responsible for these compound ratio dissimilarities; however, the associated compound “hump” diagnostic in chromatograms (Peters et al., 2005b) is not observed for any samples.

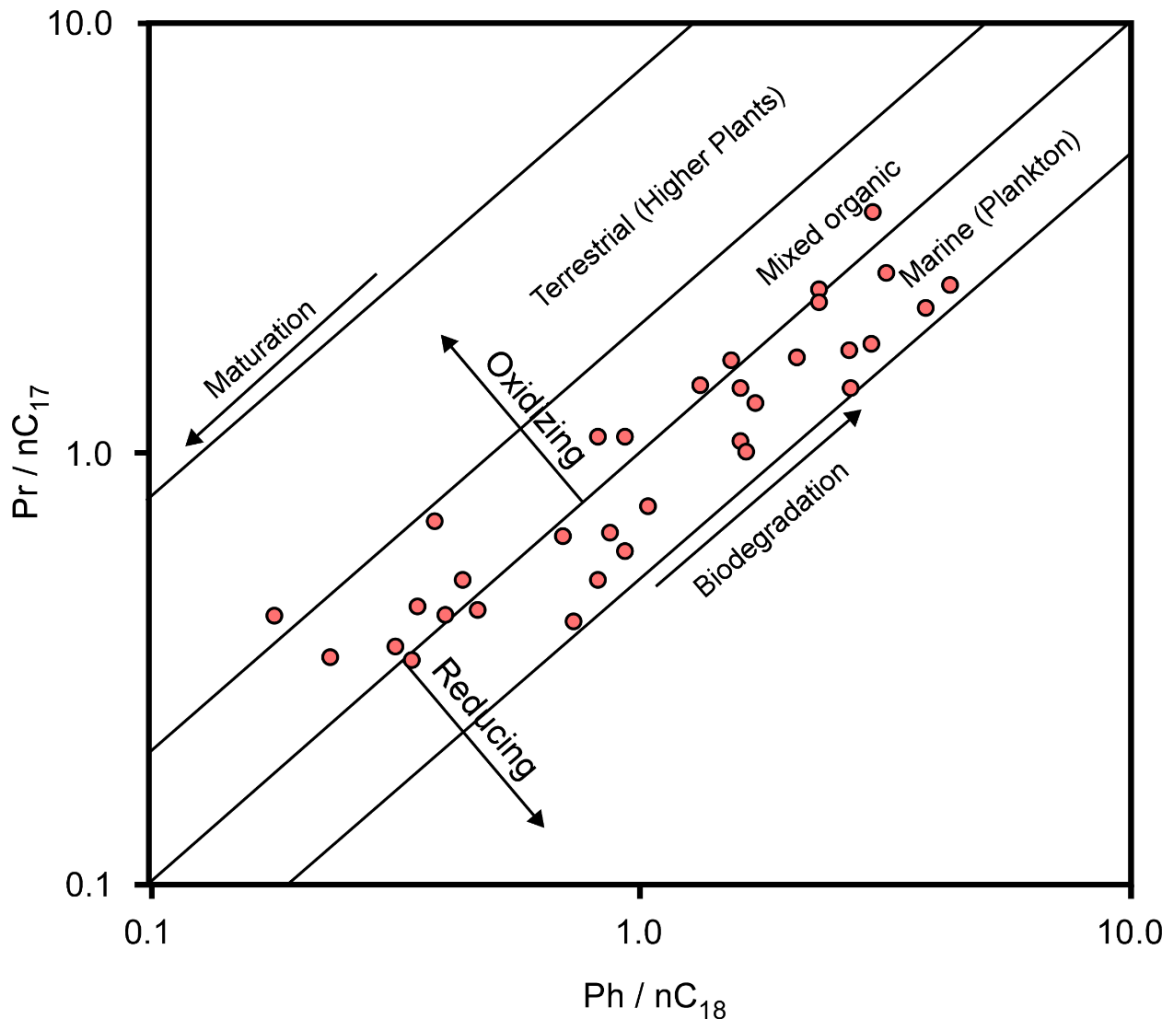


Figure 13. Cross-plotted relationships of Pristane and Phytane to their respective closest n-alkane.

Because other proxies strongly and consistently suggest that the source of OM across the WCSB is consistently marine, graphical deviation perpendicular to the $Y=X$ line on Figure 13 is attributed to variable redox conditions (Peters et al., 2005b). Locations 2, 3, 4, 5, 6(a), 9, 13(b), and 20(b) suggest the most reducing conditions relative to other locations. These agree with redox element proxies that suggest oxygen-limitation in those northern locations in the Peace River Embayment and location #9. Figure 13 suggests oxidizing conditions for location 22, but all other redox element ratios except V/Mo indicate anoxia for samples 22A and 22B, so oxygen depletion is more

likely. Inconsistencies with the various proxies illustrate the importance of multi-proxy integration to best characterize paleoceanographic conditions. These ratios are ambiguous with respect to the remaining locations.

Pristane/Phytane

The Pristane/Phytane ratio (Pr/Ph) has been broadly applied to interpret depositional redox conditions, but is most confidently interpreted in thermally immature samples (Peters et al., 2005b). Immature ($T_{max} < 430$ °C) locations north of location 11 have overall lower ratio values (0.6-1.4) relative to more southerly locations (1.4-1.7) and suggest that oxygen was more limited to the north. Peters et al. (2005b) suggests that Pr/Ph greater than 3.0 is indicative of immature terrestrial OM and less than 0.8 as indicative of anoxic carbonate or hypersaline conditions. The Pr/Ph ratio was less than 0.8 for 3A and 4B, and suggests deposition in an anoxic environment that was carbonate-rich or hypersaline (Peters et al., 2005b). Several samples are immature (based on T_{max}) from different locations, but no values are greater than 3.0, suggesting that no locations have a significant portion of terrestrial OM. Given the sufficient number of low maturity samples (15 samples $T_{max} < 430$ °C) and that only two samples fall outside of the obscuring Pr/Ph range, samples tell us that neither anoxia from hypersalinity nor immature terrestrial OM are prevalent in the Exshaw Shale Member. The total n-alkanes ($RC_{Alkanes}$) for each sample relative to the other samples in the population may also be useful for spatial characterization; higher values are achieved through enhanced preservation, dominant terrestrial source, low thermal maturity, or a combination (Peters et al., 2005b). However, no spatial trend or relationship with another variable could be identified to explain differing abundances between samples or locations. There does not

appear to be any trend that correlates with either bathymetry, thermal maturity or elemental concentration. The highest value sample, 20B, is the same sample that has the highest biomarker abundance, high silicon, low aluminum, low TOC and dark color. This sample was recovered as rubble with conchoidal fracturing and is likely chert.

HI vs OI

The van Krevelen diagram (Van Krevelen, 1993) comparing the atomic ratios of oxygen and hydrogen to carbon has been widely used to characterize organic matter in both modern and ancient environments (Espitalié et al., 1977; Tissot et al., 1974). For source rock evaluations, CO₂ and C-H bonds in OM detected by Rock-Eval pyrolysis are used to create a *pseudo* (or “*modified*”) van Krevelen diagram (Espitalié et al., 1977), by replacing the traditional H/C and O/C with Hydrogen Index (HI) and Oxygen Index (OI) gathered through Rock-Eval. Three groups emerge by plotting samples on this diagram, (Figure 14): 1) low OI, high HI; 2) low OI, low HI; 3) high OI, low HI. Samples 18A, 18B and 19A fall outside of these groups but occur on kerogen pathways between groups 1 and 2. Locations 21, 22, and 16 plot low in the overmature field for rock with high TOC.

Pseudo van Krevelen Plot

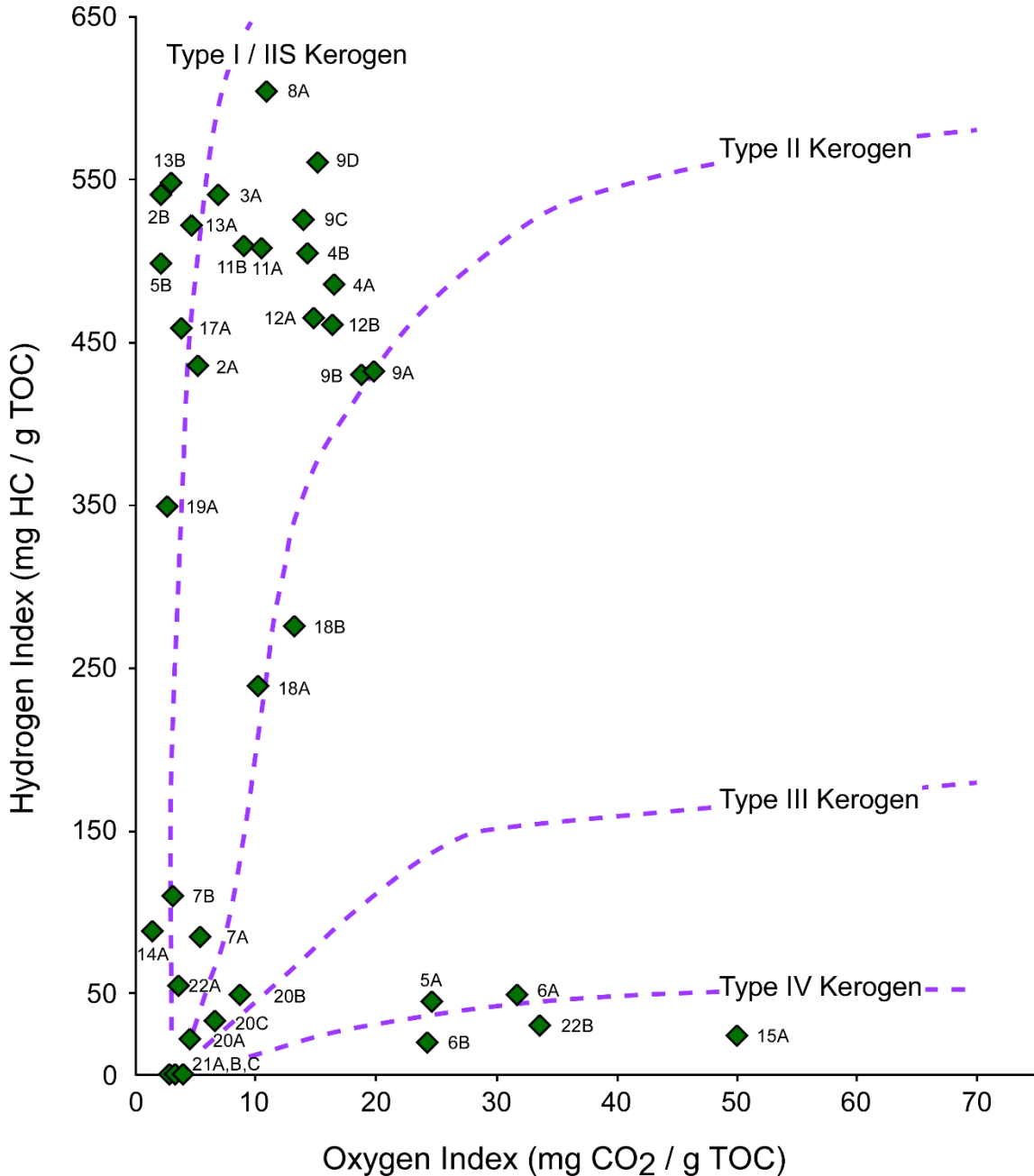


Figure 14. Pseudo van Krevelen diagram plotting one point per each sample. A True van Krevelen diagram plots measured abundances of H-C bonds and O-C bonds, while a “pseudo” van Krevelen diagram plots Oxygen Index and Hydrogen Index which are different measurements that provide similar information about the hydrocarbons present. Kerogen type pathways are generalized and accepted trajectories (Peters, 1986), and true trajectories may be slightly different for a given formation. Maturity increases along the pathways toward the origin (Peters, 1986). Note that each kerogen pathway is a broad band centered on each dotted line, not the spaces between dotted lines. Sample 16A is outside of plot area (HI: 81.25, OI: 187.5).

Traditional interpretation of data distributions on Figure 14 suggest that group 1 is immature Type I and Type II kerogen, group 2 is mature kerogen (possibly of same origin as group 1) and group 3 is Type IV (spent) kerogen. Many of the points plot along the Type I kerogen pathway (samples with both H.I. > 300 and O.I. < 15), and traditionally indicate that the organic material is lacustrine algal biomass; however, given the high sulfur content of the Exshaw Shale Member, it is more likely Type IIS. Type IIS kerogen is Type II kerogen with organic sulfur derived from marine planktonic biomass. Type IIS has initially high HI and low OI due to deposition under reducing conditions. Sulfur substitutes for oxygen in the kerogen, and the removal of oxygen results in samples that plot along the Type I kerogen pathway as Type IIS of marine origin (Orr, 1986). Based upon mechanical and biological sedimentary features, previous studies agree that the Exshaw Formation was deposited in a marine setting (Caplan and Bustin, 2001; Richards et al., 1994; Robison, 1995; Smith and Bustin, 2000). Studies undertaking petrographic analysis of kerogen structures found little evidence for terrestrial organic matter in Exshaw Formation samples and concluded that the majority of OM within the Exshaw is of planktonic marine origin (Caplan and Bustin, 1996, 1998, 2001; Robison, 1995). Outcrop samples often have diminished S1 and S2 peaks due to weathering (Peters, 1986) that decreases HI and may contribute to the low S1, S2 and HI values despite the high TOC observed at Crowsnest Pass (22A, 22B) and Jura Creek (21A, 21B, 21C). However, location 20 samples from a subsurface core have similar values for S1, S2 and HI but are not from an outcrop. This suggests that thermal overmaturity primarily influences low HI.

Source Rock Attributes

Rock-Eval Parameters

TOC concentration is reported in Table 2, and the relationship between S2 and TOC provides a quantitative measure of kerogen quality (Figure 15). This is an important source-rock consideration because high TOC with low S2 indicate that although the rock has OM, it isn't in the form of producible hydrocarbons (Carvajal-Ortiz and Gentzis, 2015; Dembicki Jr, 2009; McCarthy et al., 2011; Peters et al., 2005a). Half of all shale samples analyzed by Rock-Eval (19/37) have "excellent" quality, and "excellent" quality coincides with samples across the Peace River Embayment (locations 2, 3, 4) and Madison shelf (locations 8, 9, 11, 12 and possibly 17). "Poor" quality samples (14/37) are not restricted to a specific geographic region. The Jura Creek (location 21) and Crowsnest (location 22) outcrops exhibit similar "excellent" TOC and "poor" S2, but S2 for Crowsnest Pass is two orders of magnitude greater than S2 at Jura Creek. The Jura Creek samples are essentially void of remaining hydrocarbons. The kerogen qualities of Exshaw Shale Member samples appear to form two primary groupings, each with a similar slope but with the upper "good-excellent" group having an order of magnitude greater remaining hydrocarbon potential in comparison with the lower "poor-good" group at a given TOC value (Figure 15). However, no parameters in the elemental data nor Rock-Eval data have strong Pearson's or Spearman's Rho correlations to highlight a relationship and explain this grouping. The limiting factor for kerogen quality in the Exshaw Shale Member samples is S2. Since only four samples have less than "good" TOC (<1wt.%), it appears that basing an exploration strategy on locating intervals rich in

OM is insufficient. Rather, exploration risk is reduced by accounting for both high OM content and high S2 values.

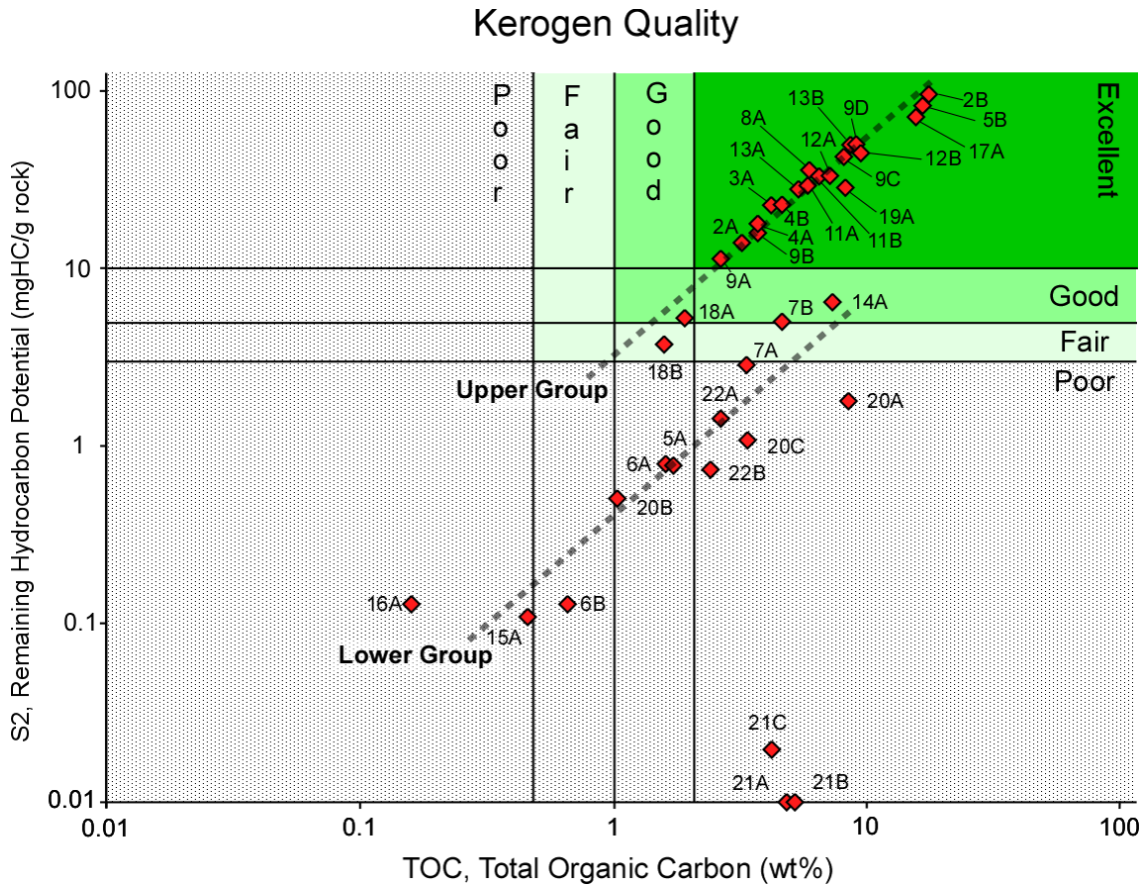


Figure 15. Kerogen quality cross plot of S2 vs TOC. “Poor”, “Fair”, “Good”, and “Excellent” are designations of source rock generation potential based on commonly accepted value thresholds for S2 and TOC (Dembicki Jr, 2009; McCarthy et al., 2011; Peters et al., 2005a)

Most of the locations with samples having high TOC but low S2 are along the deformation belt associated with the highest thermal maturity (Creaney and Allan, 1990; Richards et al., 1994; Robison, 1995). The difference in S2 values from the outcrop samples with similarly “excellent” TOC imply more thermal alteration at the northern location (Jura Creek, i.e., 21A, B, C) than the southern (Crowsnest Pass, i.e., 22A, B). This is significant because it implies that subsurface Exshaw Shale Member reservoir

potential may vary significantly over short distances along strike and away from the deformed belt.

Thermal maturity is reflected in T_{max} , the temperature of maximum hydrocarbon generation during experimental pyrolysis (the maximum of the S2 peak), with higher T_{max} values inferred to mean the rock was previously heated to a higher *in situ* temperature. T_{max} is most useful in categorizing samples from the same region into the standard thermal alteration designations of “immature,” “mature” and “overmature” as pertains to potential hydrocarbon generative status. The designations for all study area locations range from immature (17 of 37 samples $T_{max} < 430$ °C) to dry-gas overmature (6 of 37 samples $T_{max} > 480$ °C) with most classified as oil mature (13 of 37 samples T_{max} of 430-460 °C). Only 1 sample is categorized within the wet gas zone (T_{max} 460-480 °C). There are disagreements of 10 °C or more between same-core samples at locations 5, 9, 13 and 20 within the Exshaw Shale Member that cannot be explained by any lithologic or organic features revealed through XRF or Rock-Eval analyses. This is possibly the result of differences in hydrocarbon bonding in the kerogen from differing organic matter preservation or other unknown factors. The geographic distribution of T_{max} values in this study extends the area of oil maturity northward relative to published thermal gradients (Creaney and Allan, 1990; Robison, 1995; Rokosh et al., 2012) with notable exceptions (Figure 16). Locations 5 and 6 are within a region designated as thermally immature in previous studies but are classified as oil mature ($T_{max} > 430$ °C) based upon data within this study. This may indicate that thermal maturity extends farther north in central Alberta than is currently believed. Locations 5 and 6 may have been

exposed to localized high heat flow in addition to the thermal alteration attributed to regional tectonics.

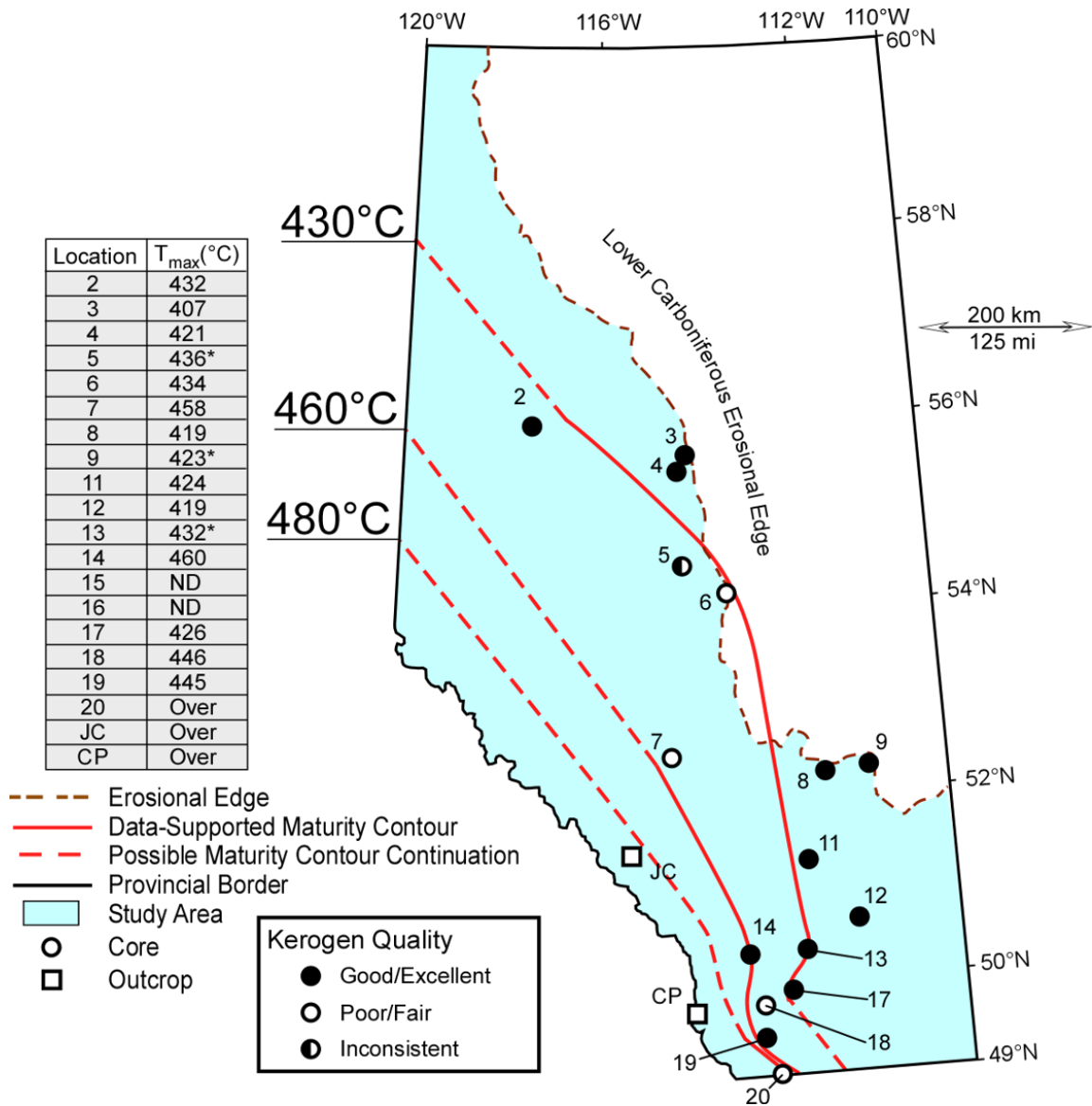


Figure 16. Thermal maturity (T_{max}) contours for analyzed locations across the study area. A value of “ND” indicates that a reliable T_{max} value could not be defined because of an unresolvable S₂ maxima. A value of “Over” indicates an ambiguous, low-confidence S₂ peak due to over maturity (Peters, 1986). *Locations 4, 5, 9 and 13 each have T_{max} values in disagreement with one or more samples at their location. The most likely value was used and is based upon shape of the S₂ peak and proximity to locations with confident values.

Knowing that kerogen for the Exshaw Shale Member is primarily Type IIS may have an impact on Tmax interpretations for exploration since shale reservoirs high in organic sulfur begin to generate oil at a lower thermal maturity than rocks with lower organic sulfur content due to the relative lability of sulfur-carbon bonds in the kerogen (Baskin and Peters, 1992; Dembicki Jr, 2009; Orr, 1986). Baskin and Peters (1992) determined that the Tmax of peak oil generation remains the same regardless of sulfur content but defined reduced Tmax thresholds for the onset of generation depending on kerogen sulfur content. Although the study dataset does not isolate the kerogen portion in samples for direct comparison to the Tmax generative thresholds of Baskin and Peters (1992), the sulfur content of the samples suggests that the Tmax of hydrocarbon generation may be lower than typical for a shale reservoir.

Maturity-related Biomarkers

The %22S, %Ts and Ts/Hop generally agree with the Tmax values in this study that indicate decreasing thermal maturity with greater distance from the deformation belt (Table 4). Sterane isomers suggest a group of samples that are immature, and a second group that are at least oil mature (Figure 17). All samples within the immature group correspond with Tmax values less than 430 °C. Samples with higher Tmax values are distributed graphically along a continuum ranging from immature to mature on Figure 17. There are, however, several immature or oil mature samples that do not have these sterane isomers in detectable concentrations.

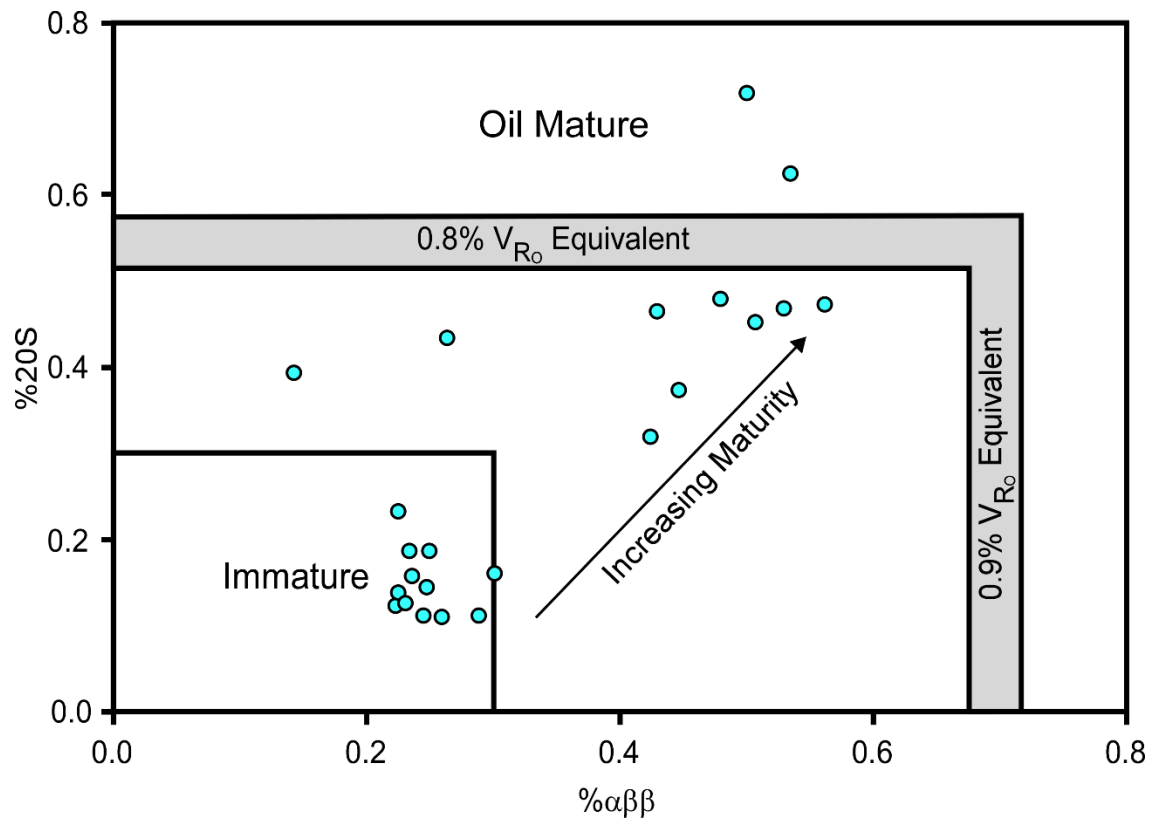


Figure 17. Crossplot of sterane ratios that estimate thermal maturity (Peters et al., 2005b).

Because OM is likely of marine origin within the study sample set, the OM does not start with odd-number or long-chain carbon predominance and OEP and CPI do not offer much information on thermal maturity (Figure 12), i.e., since they estimate maturity by decreases in the proportions of each. Nor/Hop has a specific usage and suggests that only one sample (20B) is from anoxic carbonate. Sample 20B is chert of a possible biogenic origin. The other samples are either non-carbonate, accumulated in anoxic conditions, or both. The %22S, %Ts and Ts/Hop correlate with Tmax estimations indicating increasing thermal immaturity with greater distance from the deformation belt (Table 4).

CHAPTER FIVE

Conclusions

1. This study presents new data on whole-rock elemental chemistry and Rock-Eval pyrolysis parameters along with organic geochemistry of lipid extracts from 20 Exshaw Shale Member locations on a regional scale for the OM-rich shale member of the Exshaw Formation across the province of Alberta.
2. Elemental and biomarker proxies suggest that most of the basin was not consistently euxinic or anoxic throughout deposition of the Exshaw Shale Member. More likely, intermittent anoxia or suboxia occurred locally in response to intensified periods of upwelling rather than basin-wide waterbody restriction or global changes in ocean circulation. Periods of oxygen-limited conditions are indicated by laminated bedding, high OM preservation, and several elemental and molecular proxies. Redox element ratios and biomarker ratios suggest that the Peace River Embayment and Prophet Trough may have been subjected to more intense and/or more frequent oxygen-limitation than the cratonic platform.
3. The Exshaw Shale Member is thicker than reported by most studies (4-5.5 m average in contrast to 3 m average). The Exshaw Shale Member is laminated in most locations, but burrowing, skeletal fragments and massive bedding are occasionally observed. Core observations confirm accumulation in shallow-water shelf to distal shelf-slope depositional environments.

4. Biomarker and pyrolysis data suggest that kerogen is dominantly oil-prone Type II and Type IIS kerogen from marine plankton-derived OM with moderate organic sulfur content. There is no evidence from GC-MS chromatograms or biomarker ratios to suggest widespread biodegradation.
5. Tmax, TOC, and S2 values agree that most rock across the basin is thermally mature for hydrocarbon generation, with the exception of immature locations to the east or north. The southwest portion of Alberta is overmature but may have the most variability of any region due to lithologic differences along the depositional shelf edge. Biomarker and pyrolysis data agree that the Exshaw Shale Member ranges in thermal maturity from immature (just below the oil window) to overmature (within the dry gas window), with increasing thermal maturity towards the Laramide deformation zone of southwest Alberta. In general, indicators of thermal maturity from the present study are in agreement with previous studies.
6. The moderate sulfur content of many Exshaw Shale Member samples suggests additional study is needed to resolve the relationship between Tmax temperatures and the onset of oil generation; Tmax maturity windows for sulfur-enriched organic-rich mudrocks may underestimate the true thermal maturity of hydrocarbon yield.

REFERENCES

- Abousou, A., V. Lamoureux-Var, T. Wagner, D. Pillot, I. Kowalewski, C. Marz, B. Garcia, and B. Doligez, (2018), Pyritic sulphur and organic sulphur quantification in organic rich sediments using Rock-Eval 7S: First EAGE/IFPEN Conference on Sulfur Risk Management in E&P, Rueil-Malmaison, France.
- Adams, J., S. Larter, B. Bennett, H. Huang, J. Westrich, and C. v. Kruisdijk, (2013), The Dynamic Interplay of Oil Mixing, Charge Timing, and Biodegradation in Forming the Alberta Oil Sands: Insights from Geologic Modeling and Biogeochemistry, *in* F. J. Hein, D. Leckie, S. Larter, and J. R. Suter, eds., AAPG Studies in Geology 64: Heavy-oil and oil-sand petroleum systems in Alberta and beyond, p. 23-102.
- Algeo, T. J., T. W. Lyons, R. C. Blakey, and D. J. Over, (2007), Hydrographic conditions of the Devonian–Carboniferous North American Seaway inferred from sedimentary Mo–TOC relationships: Palaeogeography, Palaeoclimatology, Palaeoecology v. 256, p. 204-230.
- Algeo, T. J., and H. Rowe, (2012), Paleoceanographic applications of trace-metal concentration data: Chemical Geology v. 324, p. 6-18.
- Arthur, M. A., and B. B. Sageman, (1994), Marine black shales: depositional mechanisms and environments of ancient deposits: Annual Review of Earth and Planetary Sciences v. 22, p. 499-551.
- Baioumy, H., and B. Lehmann, (2017), Anomalous enrichment of redox-sensitive trace elements in the marine black shales from the Duwi Formation, Egypt: evidence for the late Cretaceous Tethys anoxia: Journal of African Earth Sciences v. 133, p. 7-14.
- Baskin, D. K., and K. E. Peters, (1992), Early generation characteristics of a sulfur-rich Monterey kerogen: AAPG Bulletin v. 76, p. 1-13.
- Berbesi, L. A., R. di Primio, Z. Anka, B. Horsfield, and D. K. Higley, (2012), Source rock contributions to the Lower Cretaceous heavy oil accumulations in Alberta: A basin modeling study: AAPG Bulletin v. 96, p. 1211-1234.
- Bourbonniere, R. A., and P. A. Meyers, (1996), Sedimentary geolipid records of historical changes in the watersheds and productivities of Lakes Ontario and Erie: Limnology and Oceanography v. 41, p. 352-359.
- Bray, E., and E. Evans, (1961), Distribution of n-paraffins as a clue to recognition of source beds: Geochimica et Cosmochimica Acta v. 22, p. 2-15.

- Brumsack, H.-J., (2006), The trace metal content of recent organic carbon-rich sediments: implications for Cretaceous black shale formation: *Palaeogeography, Palaeoclimatology, Palaeoecology* v. 232, p. 344-361.
- Calvert, S. E., and T. F. Pedersen, (1993), Geochemistry of recent oxic and anoxic marine sediments: Implications for the geological record: *Marine geology* v. 113, p. 67-88.
- Caplan, M. L., (1997), Factors influencing the formation of organic-rich sedimentary facies: Examples from the Devonian-Carboniferous Exshaw Formation, Alberta, Canada: Ph.D. Dissertation, University of British Columbia, 707 p.
- Caplan, M. L., and M. R. Bustin, (1996), Factors governing organic matter accumulation and preservation in a marine petroleum source rock from the Upper Devonian to Lower Carboniferous Exshaw Formation, Alberta: *Bulletin of Canadian Petroleum Geology* v. 44, p. 474-494.
- Caplan, M. L., and M. R. Bustin, (1998), Palaeoceanographic controls on geochemical characteristics of organic-rich Exshaw mudrocks: role of enhanced primary production: *Organic Geochemistry* v. 30, p. 161-188.
- Caplan, M. L., and M. R. Bustin, (1999), Devonian–Carboniferous Hangenberg mass extinction event, widespread organic-rich mudrock and anoxia: causes and consequences: *Palaeogeography, Palaeoclimatology, Palaeoecology* v. 148, p. 187-207.
- Caplan, M. L., and M. R. Bustin, (2001), Palaeoenvironmental and palaeoceanographic controls on black, laminated mudrock deposition: example from Devonian–Carboniferous strata, Alberta, Canada: *Sedimentary Geology* v. 145, p. 45-72.
- Carvajal-Ortiz, H., and T. Gentzis, (2015), Critical considerations when assessing hydrocarbon plays using Rock-Eval pyrolysis and organic petrology data: Data quality revisited: *International Journal of Coal Geology* v. 152, p. 113-122.
- Creaney, S., and J. Allan, (1990), Hydrocarbon generation and migration in the Western Canada Sedimentary Basin: Geological Society, London, Special Publications v. 50, p. 189-202.
- Creaney, S., and J. Allan, (1991), Oil families of the Western Canada Basin: *Bulletin of Canadian Petroleum Geology* v. 39, p. 107-122.
- Creaser, R. A., P. Sannigrahi, T. Chacko, and D. Selby, (2002), Further evaluation of the Re-Os geochronometer in organic-rich sedimentary rocks: a test of hydrocarbon maturation effects in the Exshaw Formation, Western Canada Sedimentary Basin: *Geochimica et Cosmochimica Acta* v. 66, p. 3441-3452.

- Dean, W. E., and M. A. Arthur, (1989), Iron-sulfur-carbon relationships in organic-carbon-rich sequences I: Cretaceous Western Interior Seaway: *American Journal of Science* v. 289, p. 708-743.
- Dembicki Jr, H., (2009), Three common source rock evaluation errors made by geologists during prospect or play appraisals: *AAPG Bulletin* v. 93, p. 341-356.
- Driskill, B., J. Pickering, and H. Rowe, (2018), Interpretation of high resolution XRF data from the Bone Spring and Upper Wolfcamp, Delaware Basin, USA: *Unconventional Resources Technology Conference*, 2861-2888.
- Espitalié, J., M. Madec, B. Tissot, J. Mennig, and P. Leplat, (1977), Source rock characterization method for petroleum exploration: Paper presented at the *Offshore Technology Conference*, Houston, Texas, May 1977.
- Fowler, M. G., (2001), Devonian hydrocarbon source rocks and their derived oils in the Western Canada Sedimentary Basin: *Bulletin of Canadian Petroleum Geology* v. 49, p. 117-148.
- Hatch, J., and J. Leventhal, (1992), Relationship between inferred redox potential of the depositional environment and geochemistry of the Upper Pennsylvanian (Missourian) Stark Shale Member of the Dennis Limestone, Wabaunsee County, Kansas, USA: *Chemical Geology* v. 99, p. 65-82.
- Kaiser, S. I., M. Aretz, and R. T. Becker, (2016), The global Hangenberg Crisis (Devonian–Carboniferous transition): review of a first-order mass extinction: *Geological Society, London, Special Publications* v. 423, p. 387-437.
- Karavas, F. A., C. L. Riediger, M. G. Fowler, and L. R. Snowdon, (1998), Oil families in Mannville Group reservoirs of southwestern Alberta, Western Canada Sedimentary Basin: *Organic Geochemistry* v. 29, p. 769-784.
- Klemme, H., and G. F. Ulmishek, (1991), Effective petroleum source rocks of the world: stratigraphic distribution and controlling depositional factors: *AAPG Bulletin* v. 75, p. 1809-1851.
- Liu, J., and T. J. Algeo, (2020), Beyond redox: control of trace-metal enrichment in anoxic marine facies by watermass chemistry and sedimentation rate: *Geochimica et Cosmochimica Acta*, p. 1-22.
- Macqueen, R. W., and C. A. Sandberg, (1970), Stratigraphy, age, and interregional correlation of the Exshaw Formation, Alberta Rocky Mountains: *Bulletin of Canadian Petroleum Geology* v. 18, p. 32-66.
- Martin, K. G., and T. R. Carr, (2020), Developing a quantitative mudrock calibration for a handheld energy dispersive X-ray fluorescence spectrometer: *Sedimentary Geology* v. 398, p. 1-11.

- Martinez, A. M., D. L. Boyer, M. L. Droser, C. Barrie, and G. D. Love, (2019), A stable and productive marine microbial community was sustained through the end-Devonian Hangenberg Crisis within the Cleveland Shale of the Appalachian Basin, United States: *Geobiology* v. 17, p. 27-42.
- McCarthy, K., K. Rojas, M. Niemann, D. Palmowski, K. Peters, and A. Stankiewicz, (2011), Basic petroleum geochemistry for source rock evaluation: *Oilfield Review* v. 23, p. 32-43.
- Meijer Drees, N., and D. Johnston, (1996), Famennian and Tournaisian biostratigraphy of the Big Valley, Exshaw and Bakken formations, southeastern Alberta and southwestern Saskatchewan: *Bulletin of Canadian Petroleum Geology* v. 44, p. 683-694.
- Orr, W. L., (1986), Kerogen/asphaltene/sulfur relationships in sulfur-rich Monterey oils: *Organic Geochemistry* v. 10, p. 499-516.
- Parrish, J. T., (1982), Upwelling and petroleum source beds, with reference to Paleozoic: *AAPG Bulletin* v. 66, p. 750-774.
- Peters, K. E., (1986), Guidelines for evaluating petroleum source rock using programmed pyrolysis: *AAPG Bulletin* v. 70, p. 318-329.
- Peters, K. E., C. C. Walters, and M. J. Moldowan, (2005a), *The Biomarker Guide* v. 1: New York, Cambridge University Press, 471 p.
- Peters, K. E., C. C. Walters, and M. J. Moldowan, (2005b), *The Biomarker Guide* v. 2: New York, Cambridge University Press, 684 p.
- Pisarzowska, A., M. Rakociński, L. Marynowski, M. Szczerba, M. Thoby, M. Paszkowski, M. C. Perri, C. Spalletta, H.-P. Schönlaub, N. Kowalik, and M. Gereke, (2020), Large environmental disturbances caused by magmatic activity during the Late Devonian Hangenberg Crisis: *Global and Planetary Change* v. 190, p. 1-24.
- Qiao, J., A. Baniasad, L. Zieger, C. Zhang, Q. Luo, and R. Littke, (2021), Paleo-depositional environment, origin and characteristics of organic matter of the Triassic Chang 7 Member of the Yanchang Formation throughout the mid-western part of the Ordos Basin, China: *International Journal of Coal Geology* v. 237, p. 1-22.
- Richards, B. C., (1989), Upper Kaskaskia sequence: uppermost Devonian and lower Carboniferous, *in* B. D. Ricketts, ed., *Western Canada Sedimentary Basin: A Case History*, CSPG Special Publications, p. 165-201.

- Richards, B. C., J. E. Barclay, D. Bryant, C. M. Henderson, A. Hartling, R. C. Hinds, and F. Trollope, (1994), Carboniferous Strata of the Western Canada Sedimentary Basin (Chapter 14), *in* G. D. Mossop, and I. Shetsen, eds., Geological Atlas of the Western Canada Sedimentary Basin, Canadian Society of Petroleum Geologists and Alberta Research Council, p. 221-250.
- Richards, B. C., and A. C. Higgins, (1988), Devonian-Carboniferous boundary beds of the Palliser and Exshaw formations at Jura Creek, Rocky Mountains, southwestern Alberta, *in* N. J. McMillan, A. F. Embry, and D. J. Glass, eds., Devonian of the World: Proceedings of the 2nd International Symposium on the Devonian System - CSPG Memoir 14, Volume II: Sedimentation, CSPG Special Publications, p. 399-412.
- Rimmer, S. M., (2004), Geochemical paleoredox indicators in Devonian–Mississippian black shales, Central Appalachian Basin (USA): Chemical Geology v. 206, p. 373-391.
- Robison, V. D., (1995), The Exshaw Formation: a Devonian/Mississippian hydrocarbon source in the Western Canada Basin, *in* B. J. Katz, ed., Petroleum Source Rocks: Casebooks in Earth Sciences, Springer, Berlin, Heidelberg, p. 9-24.
- Rokosh, C., S. Lyster, S. Anderson, A. Beaton, H. Berhane, T. Brazzoni, D. Chen, Y. Cheng, T. Mack, and C. Pana, (2012), Summary of Alberta’s shale- and siltstone-hosted hydrocarbons: Energy Resources Conservation Board, ERCB/AGS Open File Report 2012-06, 180 p.
- Ross, D. J. K., and R. M. Bustin, (2009), Investigating the use of sedimentary geochemical proxies for paleoenvironment interpretation of thermally mature organic-rich strata: Examples from the Devonian–Mississippian shales, Western Canadian Sedimentary Basin: Chemical Geology v. 260, p. 1-19.
- Rowe, H., N. Hughes, and K. Robinson, (2012), The quantification and application of handheld energy-dispersive x-ray fluorescence (ED-XRF) in mudrock chemostratigraphy and geochemistry: Chemical Geology v. 324, p. 122-131.
- Savoy, L. E., (1990), Sedimentary record of Devonian-Mississippian carbonate and black shale systems, southernmost Canadian Rockies and adjacent Montana: Facies and processes: Ph.D. Dissertation, Syracuse University, ProQuest Dissertations Publishing, 226 p.
- Savoy, L. E., (1992), Environmental record of Devonian-Mississippian carbonate and low-oxygen facies transitions, southernmost Canadian Rocky Mountains and northwesternmost Montana: Geological Society of America Bulletin v. 104, p. 1412-1432.

- Savoy, L. E., and E. W. Mountjoy, (1995), Cratonic-margin and Antler-age foreland basin strata (Middle Devonian to Lower Carboniferous) of the southern Canadian Rocky Mountains and adjacent plains, *Stratigraphic Evolution of Foreland Basins*, SEPM Special Publication No. 52, Society for Sedimentary Geology, p. 213-231.
- Scalan, E. S., and J. E. Smith, (1970), An improved measure of the odd-even predominance in the normal alkanes of sediment extracts and petroleum: *Geochimica et Cosmochimica Acta* v. 34, p. 611-620.
- Scotese, C. R., and W. S. McKerrow, (1990), Revised world maps and introduction: Geological Society, London, *Memoirs* v. 12, p. 1-21.
- Scott, C., J. F. Slack, and K. D. Kelley, (2017), The hyper-enrichment of V and Zn in black shales of the Late Devonian-Early Mississippian Bakken Formation (USA): *Chemical Geology* v. 452, p. 24-33.
- Shanmugam, G., (1985), Significance of coniferous rain forests and related organic matter in generating commercial quantities of oil, Gippsland Basin, Australia: *AAPG Bulletin* v. 69, p. 1241-1254.
- Smith, M. G., and M. R. Bustin, (2000), Late Devonian and Early Mississippian Bakken and Exshaw black shale source rocks, Western Canada Sedimentary Basin: A Sequence Stratigraphic Interpretation: *AAPG Bulletin* v. 84, p. 940-960.
- Smith, M. G., R. M. Bustin, and M. L. Caplan, (1995), Sequence stratigraphy of the Bakken and Exshaw formations: a continuum of black shale formations in the Western Canada Sedimentary Basin: *Montana Geological Society: Seventh International Williston Basin Symposium*, p. 399-409.
- Steiner, S., and P. L. Grzegorz, (2016), Interpreting Total organic carbon TOC in source rock oil plays: Abu Dhabi International Petroleum Exhibition and Conference, p. 1-18, Abu Dhabi, UAE.
- Tissot, B., B. Durand, J. Espitalie, and A. Combaz, (1974), Influence of nature and diagenesis of organic matter in formation of petroleum: *AAPG Bulletin* v. 58, p. 499-506.
- Tribovillard, N., T. J. Algeo, T. Lyons, and A. Riboulleau, (2006), Trace metals as paleoredox and paleoproductivity proxies: an update: *Chemical Geology* v. 232, p. 12-32.
- Van Krevelen, D., (1993), *Coal: typology-physics-chemistry-constitution*: Netherlands, Elsevier Science Publishers, 1000 p.
- Vinci-Technologies, (2021), Rock-Eval 7S Data Sheet, Guidebook from the instrument manufacturer, URL: [vinci-technologies.com/images/contenu/documents/AMONT/RE7S%20Data%20Sheet.pdf](https://www.vinci-technologies.com/images/contenu/documents/AMONT/RE7S%20Data%20Sheet.pdf).

- Vine, J. D., and E. B. Tourtelot, (1970), Geochemistry of black shale deposits- A summary report: *Economic Geology* v. 65, p. 253-272.
- Wedepohl, K., (1971), Environmental Influences on the Chemical Composition of Shales and Clays, *in* L. H. Ahrens, F. Press, S. K. Runcorn, and H. C. Urey, eds., *Physics and Chemistry of the Earth*: New York, Pergamon Press, Ltd., p. 307-333.
- Wedepohl, K., (1995), The composition of the continental crust: *Geochimica et Cosmochimica Acta* v. 59, p. 1217-1232.
- Wheeler, H. E., (1963), Post-Sauk and pre-Absaroka Paleozoic stratigraphic patterns in North America: *AAPG Bulletin* v. 47, p. 1497-1526.
- Witzke, B., and P. Heckel, (1988), Paleoclimatic indicators and inferred Devonian paleolatitudes of Euramerica: *Devonian of the World: Proceedings of the 2nd International Symposium on the Devonian System, CSPG Special Publications: Memoir 14*, p. 49-63.
- Witzke, B. J., (1990), Palaeoclimatic constraints for Palaeozoic palaeolatitudes of Laurentia and Euramerica: *Geological Society, London, Memoirs* v. 12, p. 57-73.
- Yang, S., (2019), Reconstruction of local and global marine paleoredox conditions during deposition of the Devonian-Mississippian Exshaw Formation (Black Shale Member) and the evaluation of hydrocarbon maturation effects: M.S. Thesis, University of Waterloo, Waterloo, Ontario, Canada, 108 p.